nature microbiology

Article

https://doi.org/10.1038/s41564-023-01527-3

Ancient dental calculus reveals oral microbiome shifts associated with lifestyle and disease in Great Britain

In the format provided by the authors and unedited

Supplementary Information

The Supplemental Information for this manuscript includes:

- Supplementary Text
- Supplementary Figures S1 to S19
- Supplementary Tables S1 to S23
    - Table S1: Sample Metadata
    - Table S2: EBC versus Sample Comparisons
    - Table S3: Sample Assigned Sequence Counts
    - Table S4: Species Filtering
    - Table S5: ChangePoint Analysis
    - Table S6: Whole British Set ADONIS tests for correlation of microbiota taxonomic data with oral geography and sampling laboratory processing at all taxonomic levels
    - Table S7: Whole British Set ADONIS tests for correlation of microbiota taxonomic data with oral geography and sampling laboratory processing at the genus level
    - Table S8: Whole British Set ADONIS tests for correlation of microbiota taxonomic data with oral geography and sampling laboratory processing at the species level
    - Table S9: Whole British Set ADONIS tests for correlation of microbiota functional data with oral geography and sampling laboratory processing
    - Table S10: Genera Relative Frequency
    - Table S11: Dominant Community Correspondence Analysis
    - Table S12: ADONIS of Culture and Health Variables For All Teeth and Molars, With Factors Based On Oral Geography Tables Accounted Into Models
    - Table S13: MapDamage Results
    - Table S14: List of Functions Identified & Analyzed in British Dataset
    - Table S15: Figure 4 Associated Dietary Function Data and Tests
    - Table S16: MoL Oral Geography ADONIS- All Levels
    - Table S17: MoL Oral Geography ADONIS- Genus Level
    - Table S18: MoL Oral Geography ADONIS Species Filtered
    - Table S19: LefSe For MoL Pathologies
    - Table S20: Mapping File Used for SourceTracker Analysis
    - Table S21: ALDEX2 Results for Functions Associated With Diet
    - Table S22: Comparison of Genera in EBCs vs Known Contaminant Taxa
    - Table S23: Tests of Whether Dominant Category is Associated with Significant Variables in Table 1

Contents

Section 1: Archaeological Context and Sample Descriptions

Time Periods

This project examined dental calculus present on the teeth of individuals who lived from the late Neolithic to the early Victorian period, although robust oral microbial communities were only obtained from individuals as old as the Bronze Age (Figure 1; ~200 BCE to 1853 CE). Samples were collected from a variety of British Museums (Table S1), although the focal point of this project was the Wellcome Osteological Research Database at the Museum of London. A total of 235 ancient human remains were sampled for this project from 27 cemeteries, and the majority dated to the Post-Roman period (post 410 CE), especially the post-Norman Invasion period (post-1066 CE).

Specific cultural periods referred to correspond to the following date ranges: Pre-Roman Britain (up to 43 CE), Roman Britain (43 CE – 410 CE), Anglo-Saxon Britain (410 – 1066 CE), Norman Britain and the Middle Ages (1066 CE – 1547 CE), Reformation (1547 CE – 1750 CE), and Industrial (1750 CE – 1900 CE).

British Sites and Individuals

Breedon On The Hill (N = 6)

Six individuals originated from Breedon on the Hill, Leicestershire, excavated by Don Brothwell. These were identified as middle Anglo-Saxon (dating to approximately 676 CE).

Eccles (N = 6)

The burials from Eccles, England, were identified as middle Anglo-Saxon. Some of these individuals were potentially infected with leprosy.

Hill of Roseisle (N = 1)

The individual from the Hill of Roseisle, Scotland, (SK 1666) was a Bronze Age male.

Hinxton (N = 9)

Nine individuals originated from Hinxton in Cambridgeshire, England, ranging from the Iron Age to the middle Anglo-Saxon period. Four were females, four males, and one was a subadult.

Isle of Lewis (N = 1)

One individual was sampled from the Isle of Lewis, Scotland (SK 1712). This individual was identified as a possible male.

Isle of Pomona (N = 1)

One female individual (SK 1669) originated from the Isle of Pomona in the Orkney region of Scotland.

Jewbury (N = 8)

Eight individuals (J4104, J2585, J2303, J2496, J4119, J2562, J4218, J2703) originated from the Jewbury cemetery in York, England. These were all dated between 1170 and 1290. Four were identified as male, three as female, and one was unknown.

Kirkhill (N = 2)

Two individuals (SK 1693, SK 1694) originated from the Kirkhill cemetery in the St Andrews region of Scotland. Both were identified as male.

Kirkwall Cathedral (N = 3)

Three individuals (SK 1699, SK 1704, SK 1701) originated from the Kirkwall Cathedral in the Orkney region of Scotland. Two of these were identified as male, and the other as unknown. All three dated to the Viking Age.

Linton (N = 3)

Three individuals (SK 308, SK 352, SK 350) originated from the Linton cemetery in Cambridge, England and dated between 690 and 900 CE to the middle Anglo-Saxon period. All three were identified as males.

Newark Bay (N = 2)

Two Viking Age individuals (69/x, 68/14) originated from the Newark Bay cemetery in Newark Bay, Scotland, excavated by Don Brothwell.

Oakington (N = 8)

Eight individuals (ACAD15553, ACAD1550, ACAD15558, ACAD15560, ACAD15576, SK 887, SK 788, SK 890) originated from the Oakington cemetery in Cambridge, England, and dated between 450 and 600 CE to the early Anglo-Saxon period. Five were identified as female, one as male, and two were unknown.

Raunds (N = 7)

Seven individuals (R5287, R5008, R5287, R5061, R5229, R5093, R5018) originated from the Rounds Cemetery in Northampton, England. These dated between 950 and 1150 CE to the Late Anglo-Saxon period. Of these, five were male and 2 were female.

Skae Brae (N = 1)

A single individual (SK 1975) was sampled from the Skae Brae cemetery in Orkney, Scotland. This individual dated to the Neolithic period and was identified as male.

St. Helens-On-the-Wall (N = 3)

Three individuals (5228, 5614, 5241) originated from the St. Helens on Wall Cemetery in York, England. These dated between 1100 and 1550 CE to the Late Medieval period. All three were identified as female.

St. Ninians Isle (N = 4)

Four individuals (1975.1.1.24, 1975.1.1.31, 1975.1.1.36B, 1975.1.1.13) originated from St. Ninian's Isle Cemetery on St. Ninian's Isle in Scotland. One was identified as male, and the other three were unknown.

Yorkshire (N = 4)

Four individuals (T82GF, 108, 45, T100) originated from the Yorkshire cemetery in York, England. These dated between 2100 and 800 BCE in the Bronze Age period.

Balintore, Scotland (N = 4)

Three individuals (1985.022, 1982.083, 1982.082) were sampled from Balintore, Ross and Cromarty, Scotland. One individual (1985.022) was revealed to be Neolithic (dated to 3370-3030 cal BCE) (Sanchez-Quinto et al. 2019) and was identified as female through genetic analyses. The remaining indivduals are thought to be Pictish.

London Sites and Individuals

The London individuals originated from nine archaeological sites from a 10-square mile section of London (16 km^2). These included monastic (Bermondsey Abbey Spital Square, Merton Priory, St. Benet Sherhog, St. Mary Graces, and St. Brides), layman (Guildhall Yard), low class (Cross Bones), and upper class (Chelsea Old Church) burials and cemeteries. All individuals were over 18 years of age and had extensive cultural and pathological data associated with them, as described in the Wellcome Osteological Research Database (WORD), including information about age and sex estimations, blood disorders, dental and vertebral anomalies and pathologies, and joint disease. More detailed information about each of these sites and individuals is available at the WORD online database[1]**.** Only metadata fields that recorded observations of the absence or presence of a trait or pathology were used. Severity measurements were collapsed to simply note presence of the trait or pathology. Any individual without an observation was excluded from analysis of that trait or pathology.

Bermondsey Abbey (N = 10)

The site of Bermondsey Abbey is located at Saint Saviour Monastic Cemetery, Bermondsey Abbey, Abbey Street, Long Walk, Southwark, London. Excavated in 1984 and 1988, the site contained a total of 201 individuals associated with the monastic order who mostly dated between 1099 and 1538 CE. 200 of the

individuals were adults, with nearly all of the identifiable individuals being males.

Chelsea Old Church (N = 11)

Chelsea Old Church is an 18th-19th century churchyard located on Old Church Street, Chelsea, London. In 2000, excavations carried out by the Museum of London Archaeological Services revealed 290 skeletons, of which 198 were analyzed. Of the 168 adults, 74 were female, 78 male, and 16 unsexed. The Chelsea population reflected a typical post medieval disease pattern (MoL Website) associated with metabolic disorders.

Cross Bones (N = 10)

Cross Bones was excavated in 1992, allowing for the recovery of 148 inhumations dating between 1800 and 1853. The site, located at Redcross Way, London, represents a post-medieval population from an area with a very poor socio-economic environment. The site contains many young individuals, with more females than males in most age categories.

Guildhall Yard (N = 10)

The Guildhall Yard site was excavated from Portland House, 72-73 Basinghall Street, London, by the Museum of London Archaeological Service between 1992 and 1997. This was a lay cemetery whose burials date between the late 11th and the early 12th century. A total of 68 individuals were analyzed. Of these, 69.1% were adults, with approximately equal numbers of males and females.

Merton Priory (N = 60)

The site of Merton Priory was excavated in the late 20th century, with the excavations revealing 738 burials dating between 1117 and 1538 CE. Most individuals were adults, and 90% of those sexed were determined to be male. The site represents a monastic cemetery population as well as lay individuals.

Spital Square (N = 23)

Spital Square, previously referred to as “St. Mary Spital”, is located on the northern side of Folgate Street in North East London. Excavations were carried out between 1985 and 1989 by the Museum of London, during which a total of 126 human remains were found, dating between 1197 and 1320. 43 were male, 23 female, and 42 were subadults. The site is associated with a hospital.

St. Benet Sherehog (N = 17)

St. Benet Sherehog was excavated between 1994 and 1996 by the Museum of London. The site is located across multiple roads in London. A total of 274 burials were excavated and 270 were analyzed, with 39 dating medieval and 235 post-medieval. The site had a similar number of males and females. The site

represents a post-medieval urban population within the city of London, dating mainly to the 16th and 17th centuries.

St. Brides (N = 6)

St. Brides is located on Farringdon Street in London and represents a population who lived in the parish between the 17th and 19th centuries. A total of 606 individuals were excavated, with 544 available for analysis. The site represents a large post-medieval population of low socioeconomic status and has a similar number of males and females.

St. Mary Graces (N = 19)

St. Mary Graces is a site excavated between 1986 and 1988 that dates between 1353 and 1538. The site is located at the former Royal Mint in East Smithfield, London. A total of 389 individuals were analyzed from 420 burials. Of the 389 skeletons, 283 were adults with 136 males and 68 females. The site is known for the closely associated catastrophic Black Death Cemetery (East Smithfield).

Modern and Other Comparative Samples

In addition to the ancient individuals analyzed in this survey, a number of other comparative samples from former studies were included in the analyses. These included Neanderthal samples from El Sidrón, Spain (2) and Spy Cave, Belgium (1) as well as a Chimpanzee sample (ACAD 12873)[2]. The modern oral samples were modern plaque (n=5)[3] and dental calculus (n=1)[2]. We also included two additional Medieval samples from Germany that were previously published by Warinner et al (2014) (Warinner_B61_MALT_ALL, Warinner_G12_MALT_ALL)[4].

Section 2: Sampling & Laboratory Procedures

Dental calculus collection

Calculus deposits are routinely found on the teeth of archaeological human remains and contain DNA from bacteria, archaea, viruses, fungi, and parasites, as well as DNA that reflects the diet and lifestyle of an individual[5–8].

Sampling strategies

Dental calculus sample collection was done using sterile procedures as previously described[8]. Specifically, gloves were donned to limit contamination from the researcher, and a sterile dental pick was used to remove dental calculus from teeth. Enamel damage was avoided by applying pressure parallel to the tooth. The largest deposit of dental calculus on a specimen was used as a sample over aluminum foil. Calculus samples were stored in labeled sterile zip seal bags and transported to the ancient DNA facility at the Australian Centre for Ancient DNA (ACAD). Information about calculus was recorded, including the

collection, collector's name, skeletal metadata, tooth type, region, and aspect, details regarding calculus (color, size, etc.), and other pertinent details.

Calculus sample size was also recorded prior to extraction. Using pixelstick, the longest length of the calculus was recorded, then the widest point perpendicular to the length measurement. These were used to calculate the area. Dental calculus sample size was not normalized. Calculus sample size was then sorted into the following bins:

Bin	*Estimated Size*
1	< 1 mm^2
2	1 - 5 mm^2
3	6 - 10 mm^2
4	10 - 15 mm^2
5	16 - 20 mm^2
6	21 - 25 mm^2
7	26 - 30 mm^2
8	> 30 mm^2

Sample preparation

Ancient samples were shipped to the Australian Centre for Ancient DNA (ACAD) at the University of Adelaide, Australia. The samples were then stored at 4°C. Prior to DNA extraction, each calculus sample was decontaminated by being placed on a sterile plastic dish and UV irradiated for 15 minutes on each side (30 minutes total), then submerged in 5% bleach (3 minutes) followed by immersion in 1 mL 80% ethanol for 1 minute to remove remaining chemicals[9,10]. The samples were then air dried for 5 minutes before being placed in a sterile 1.5 mL tube, where the calculus was pulverized by applying pressure using the side of a pair of sterilized forceps.

DNA extraction

All procedures were done in UV-treated, still air hoods located in isolated, still-air rooms within a specialized ancient DNA laboratory facility. DNA extraction was performed as previously described[2,11]. Briefly, DNA extractions were performed using an in-house silica-based method but with decreased buffer volumes (1.8 ml lysis buffer (1.6 mL 0.5 M EDTA; 200 µl SDS (10%); 20 µl proteinase (20mg/mL)) and 3 ml guanidine DNA-binding buffer). Extraction blank controls (EBCs) were included at the beginning and end

of each sample series. Each DNA extraction included two negative controls at a ratio of one negative control per seven calculus samples.

Library preparation

Shotgun metagenomic libraries were generated without enzymatic damage repair, as done previously, with forward and reverse barcodes and single end indexes[2]. Briefly, 20 µl of DNA extract was prepared by enzymatic polishing to produce blunt ended fragments before ligation of truncated barcoded Illumina adapters and the filling of gaps with adapter sequences. No template controls (NTCs) were included alongside extraction blank controls in this process. Qiagen MiniElute Reaction Clean-ups were completed after each step, and each sample underwent triplicate PCR amplification for 13 cycles (HiFi) with a full-length indexed Illumina adaptor to increase concentration while maintaining complexity. PCR products were pooled and purified with the Agencourt AMPure XP system. A 2 nM sequencing library was produced following a second round of pooling, purification, and quantification using TapeStation (agilent) and quantitative PCR (KAPA Illumina quantification kit).

Sequencing

Sequencing was performed using a high output 2 x 150 bp kit on the Illumina NextSeq.

Section 3: Data processing, quality filtering, and authentication

Data Processing Steps

Sequenced samples were converted from BCL files to FastQ files, and demultiplexed using sabre, a barcode demultiplexing and trimming tool for FastQ files[12]. Demultiplexed FASTQ files were processed using bbmerge to merge reads (5bp overlap) and Adaptor Removal[13] to remove 5' and 3' barcode and adapter sequences. Reads longer than 300 bp were discarded, as they likely represent modern contamination. A quality threshold of Q30 was applied, and reads were only included in downstream analysis if they were longer than 25 base pairs.

Taxonomic and functional identifications were identified using MALTX, a tool which was developed by the Huson lab at the University of Tuebingen-, against the NCBI nr database (2014) using default parameters[14]. We repeated the analysis to assess biases in the data originating from protein alignment by performing taxonomic assignments using MALTn against the 2017 NCBI RefSeq GCS database using the weighted LCA algorithm (0.8)[15]. MALTx and MALTn output files were converted into RMA files and uploaded to MEGAN6 Community Edition (CE) using the default LCA parameters.

MEGAN6 CE was then used to export Operational Taxonomic Units (OTUs) at the species, genus, and phylum levels using the TaxonNameToCount and summarized options.

Sample Quality Filtering

Of the 235 dental calculus samples and 24 extraction blank controls (EBCs), DNA sequences were successfully obtained from 201 of the samples (85%) and 18 of the controls (75%). With these samples, we then performed a comprehensive approach with multiple filtration steps to identify high quality samples and remove potential contaminants (Figure S3). First, we compared the ancient dental calculus samples to the EBCs. Second, we only retained samples that exceeded 100,000 assigned reads. Third, we conservatively filtered out any species that were detected within the negative controls.

Comparison to EBCs

In MEGAN6 CE, a Bray-Curtis dissimilarity matrix of samples and negative controls was generated at the genus level, and negative controls with a Bray-Curtis dissimilarity greater than 0.6 in comparison to other negative controls were excluded. Four times the standard deviation of the remaining negative controls was calculated, and any samples within this range were removed from the analysis. 14 dental calculus samples were removed because they were not significantly different from laboratory controls (i.e., <0.75 dissimilarity) (6.9%; Table S2 and Figure S1).

Minimum Assigned Sequences

Samples with fewer than 100,000 assigned sequences (i.e., sequences that were identified as a specific taxa) post-filtering were discarded to ensure accurate taxonomic reconstruction (Table S3)[16].

Species-Based Filtration

Species detected within the EBCs (n=609) were conservatively removed from all calculus samples for species-based analyses; 38.9% of all species were removed from a total of 1564 (Table S4), leaving 954 species identified in ancient British calculus samples. Due to low sequencing depth of NTCs, these control samples were not included in downstream analyses. Species within the EBCs were largely not oral in origin (Figure S4), which is likely attributed to specific laboratory sample handling, cleaning protocols, specific reagent storage and handling, and work completed within an ultraclean ancient DNA laboratory [17]. Nevertheless, strict filtering of samples may not be appropriate in all cases, and in instances where oral taxa are present in EBCs, methods, such as decontam, which model abundance-based contamination may be more appropriate[18]. To further explore the robusticity of our conservative filtering, we also completed a decontam analysis using our EBCs and found that 321 (57%) of the taxa identified as contaminant across both methods. However, decontam failed to identify many of

the species within genera that are largely determined to be contaminants in oral microbiome analyses (i.e., *Acinetobacter*), so we maintained the conservative filtering approach for this paper.

Decontam R Package

We used decontam to assess whether our species-based filtering step worked effectively. The decontam R package[18], which implements a statistical classification method to identify contaminant taxa based on their prevalence in a defined set of negative controls relative to biological samples, was used to identify and remove contaminant species using the prevalence method. For this analysis, the calculus samples were treated as biological samples, while EBCs were treated as controls. Using a stringent threshold of 0.7, a total of 321 taxa were identified as contaminants, in such that the taxa were more prevalence in laboratory control samples than within dental calculus samples. The species-based filtration step filtered out an addition 288 species found in the EBCs, and so we proceeded with the more conservative of the methods.

Verification of oral microbial composition of British Samples

To assess the overall composition of the ancient samples, we generated compositional stacked bar plots at the genus and phylum levels for both British samples and the comparative, control samples. At the phylum level, most samples were dominated by Firmicutes, Actinobacteria, Proteobacteria, and Bacterioidetes. At the genus level, most samples were dominated by *Methanobrevibacter*, *Fretibacterium*, *Streptococcus*, and *Actinomyces* (Figure S4) – all genera commonly found in the Human Oral Microbiome Database (HOMD)[19].

SourceTracker Analysis

To examine the overall microbial content of the dental calculus samples, two Sourcetracker analyses were performed. In short, this tool produces Bayesian estimates of source contributions given to a metagenomic sample based on the metagenomes of well-characterized environments.

For the first analysis, samples examined using MALTx were analyzed with SourceTracker (v1.0.1)[20], in the same fashion as described in Weyrich et al. (2017)[2]. The comparative. rma5 files for the "source" contributions were obtained from Ramirez et al 2020, Weyrich et al 2017, and Warriner et al 2014 and included samples from Ancient Calculus, Modern Calculus, Extraction blank controls (EBCs), and Soil (Table S20). The comparative sources were selected based on the following criteria: 1) data generated using Illumina shotgun sequencing; 2) in the case for calculus samples, data from independent individuals; and 3) had enough data to yield at least 1,000 counts mapped to the RefSeq database using MALTx, as observed in Weyrich, et al. 2017. The raw shotgun sequences for these source communities were bioinformatically processed in the same way as the samples in the current study. SourceTracker was ran using the default settings.

In this analysis, the majority of the genera within the British calculus samples could be contributed to the oral microbiome. We observed that 185 samples out of 186 samples had at least 50% of their microbial DNA attributed to oral sources, as well as 160 having at least 70% attributed to these oral sources, although one sample had less than 50%. In summary, this SourceTracker analysis suggest that the dental calculus samples in this study are well-preserved.

To corroborate the results, Sourcetracker (v2.0.1)[20] was also employed to assess the microbial community of the dental calculus samples based on their taxonomic profiles generated with MALTn. The comparative data for the "source" contributions included samples from studies analyzing ancient dental calculus, modern dental calculus, modern dental plaque, soil, skin, and extraction blank controls (EBCs) (Table S20). The comparative sources were selected based on the following criteria: 1) data generated using Illumina shotgun sequencing; 2) in the case for calculus samples, data from independent individuals; 3) had enough data to yield at least 1000 reads mapped to the RefSeq GCS database using MALTn. The raw shotgun sequences for these source communities were bioinformatically processed using the same methodology as the dental calculus samples in the present study.

Previous research indicates that the microbial communities between ancient dental calculus, modern dental calculus, and modern dental plaque are distinct[4,9,21]. As such, we treated these environments as separate sources. The ancient dental calculus samples came from well-preserved samples published in Eisenhofer et al. (2020)[22] and Velsko et al. (2017)[23]. Non-diseased modern dental calculus samples from Califf et al. (2017)[24] were used for the 'ModernCalculus' environment, while non-diseased plaque samples from the Human Microbiome Project (HMP) were used for the 'Plaque' environment. Soil samples from Perez et al. (2022)[25] and skin samples from Larson et al. (2022)[26] were chosen because these samples were deeply sequenced. Lastly, EBCs that were generated during the laboratory process for this project were used as an additional source.

Reads for the source samples were processed using the same bioinformatic pipeline used for the British samples. The reads were summarized to the genus level and exported to a taxon table in the BIOM format. The source samples were then combined with the British samples. Sourcetracker2 was used to calculate the source mixing proportions in the British samples (alpha1=0.01, alpha2=1.0, sink_rarefaction_depth=2000, source_rarefaction_depth=2000). Rarefaction depth of 2,000 was chosen because of the sequencing depth for the SRR17651691 sample (Table S20). This SourceTracker analysis indicated that modern plaque microbes were similar to a considerable (>50%) portion of the dental calculus microbiome in the British samples, while little with the modern dental calculus samples (3.77%). Across all samples, skin (1.71%), soil (0.11%), and EBC (0.08%) contamination contributed very little to the overall community structures (Figure S13). An additional analysis using the ancient dental calculus as the only oral source was also performed. This analysis indicated that the microbial communities in the British

dental calculus samples are very similar to previously published dental calculus communities (94.84%). As with the previous analysis, small amounts of contamination could be traced to skin (2.63%), EBCs (0.12%), soil (0.18%), and unknown (2.22%) sources (Figure S13). In summary, the results demonstrate that ancient British oral calculus samples consist of mostly oral signatures.

To further validate the preservation of the British samples, we generated a stacked-bar plot of taxa that were present at >5% total abundance across at least 80 samples to explore which species were the most prevalent in the samples and whether they were oral (Figure S13). All of the species listed can be found in the HOMD database, such as *Tannerella forsythia, Actinomyces dentalis, Fretibacterium fastiosum, Treponema socranskii, Methanobrevibacter oralis, Anaerolineaceae bacterium oral taxon 439*, and *Streptococcus sanguinis*. These results further indicate that the species in the ancient samples are predominantly oral.

Changepoint analysis

To authenticate the ancient signatures in the samples, we ran ChangePoint analysis, a program designed to assess DNA damage of unmapped DNA sequences[27]. The method relies on the differential proportions of 3' 'A' and 5' 'T' nucleotides near the ends of the DNA sequences and models the relationships between the distance from the end of the reads and the amount of deamination in a sample to determine whether there is significant damage present. To perform these analyses, we subsampled samples to 100,000 reads in order to optimize the performance of the program and then ran the Changepoint script. The results (Table S5) indicated that the EBCs, as well as six samples were, non-significant for both ends. The test value for this statistic is the result of a likelihood ratio test, and p-values are adjusted such that the false discovery rate is 0.05.

MapDamage2.0

To confirm the ChangePoint results, we also ran MapDamage2.0 on all the samples[28] using the endogenous oral references of *Actinomyces oral taxon 414, Anaerolineaceae bacterium oral taxon 439, Methanobrevibacter oralis, Streptococcus sanguinis*, and *Porphyromonas gingivalis* and the contaminant references of *Burkholderia multivorans, Comamonas testosteroni, Escherichia coli*, and *Flavobacteriaceae bacterium*. The resulting number of reads, theta, deltaD, DeltaS, Lambda, Rho, and LogLik means and standard deviations are available in Table S13. The endogenous oral species demonstrated higher average cytosine deamination probabilities than exogenous taxa (0.030 vs 0.023).

Section 4: Microbial composition analysis

Impacts of oral and sampling biases

Modern DNA research suggests that oral geography and laboratory environments can significantly impact the composition of the oral microbiome[29]. These findings have been supported by ancient DNA publications[30,31]. Therefore, we assessed the impacts of oral geography (i.e., tooth type, tooth surface, supra- vs. subgingival, maxilla vs. mandible, and left vs. right) and technical biases (sampling data, extraction group, library preparation group, in situ or loose tooth, and the surface area of the calculus sample selected for extraction (referred to as calculus sample or fragment size)) on both the taxonomic and functional compositions of our data set (Figure 2; Table S6-S9).

To assess this, we ran ADONIS tests on the following traits: 'Extraction ID', 'Library ID', Buccal versus Lingual aspects, Calculus Sample Size Bin, *in situ* versus loose tooth, right versus left oral aspects, maxillary versus mandibular aspects, sub- versus supragingival calculus, and tooth type at all taxonomy, genus, and species levels (Table S6-S8). The oral geography factors to be tested were chosen based on the literature[29,32]. For instance, sub- versus supragingival calculus samples are known to have different contents and formation processes[33].

This analysis was performed by taking the normalized ancient samples and running permutational multivariate analysis of variance using distance matrices (ADONIS) tests with 999 permutations based on Bray-Curtis distance matrices. First, each respective metadata category was filtered so that only relevant (e.g., no 'NA' or other unknown) variables were included (i.e., samples with no information were excluded). The data was then normalized to the following levels: all taxonomic assignments was normalized at 100,000, genera to 50,000, and species to 30,000 identified sequences. Metadata categories were only included if at least five individuals in each category of each metadata characteristic were available, and if a sample did not have a known value for the metadata field being tested, that sample was excluded from that specific test.

Across all teeth, extraction ID, calculus sample size, and maxilla versus mandible significantly impacted the taxonomic composition when examining all taxa, genera, and species (Table S6-8). Biases were also unique to specific taxonomic levels (e.g., supra- versus subgingival in species; Table S8) and functions (e.g., buccal vs lingual in functional composition; Table S9). As previous research suggests that tooth type may specifically contribute to oral microbial composition, we also examine composition associated with tooth type (i.e., incisors, canines, bicuspids, and molars). The molar calculus microbiome composition was associated with calculus sample size and supra versus sub-gingival location of calculus (Table S6-S9), while incisor microbiota composition was significantly influence by tooth surface (e.g., buccal versus lingual surfaces; Figure 2C), suggesting that the impacts of oral geography may differ according to the type of tooth sampled.

In addition to performing these analyses on taxonomic data, we also analyzed the functional export from MEGAN6 CE at the SEED Level 4 level (Table S9). When examining all teeth, library ID was significant, while the date sampled, buccal versus lingual, in situ versus loose tooth, and right versus left aspects were significant depending in individual tooth types (i.e., either only incisors or molars).

We also performed an identical ADONIS analysis on only the samples from the Museum of London (N = 127) to examine the impacts of oral geography when looking at individuals all residing in the same city (Tables S16-18). Unlike within the complete British dataset, tooth type emerged as a significant factor, and therefore future analyses were done by looking at a subset containing only molars. In addition to tooth type, sub versus supragingival, maxilla versus mandibular, buccal versus lingual, and calculus sample size bin were all detected as significant oral geography factors.

Therefore, we accounted for the laboratory and oral geography factors shown to be significant (above) and performed analyses in either all teeth or only molars, as molars were predominantly sampled for this study. Overall, these results indicate that laboratory processing and oral geography can significantly confound taxonomic and functional compositions in ancient dental calculus datasets.

Geographical and cultural associations

To test for geographical and cultural associations within this dataset, we assessed a host of factors related to spatial (cemetery, country, rural versus urban, north versus south, empire), temporal (pre or post Black Death, pre- post- during- Civil War, medieval or post-medieval, 300-year block periods, 400-year block periods), and cultural (class, hospital, rank, religion, sex) traits. These were analyzed by performing ADONIS tests with 999 permutations using all taxonomic classifications, genera, or species and functional levels for both all samples as well as only molars. Metadata categories were only included if at least five individuals in each category of each metadata characteristic were available, and if a sample did not have a known value for the metadata field being tested, that sample was excluded from that specific test. For each of these 8 subsets, the oral geography and sampling factors deemed significant above (Tables S6-S9) were incorporated into each test prior to the variable of interest. In cases where there were too few subgingival samples to add to the model, the variable was excluded. In addition, we also performed this analysis on only samples from London (Table 1).

Oral and systemic health associations

In addition to testing temporal, spatial, and cultural variables, we also analyzed factors associated with oral and systemic health (Table 1). Due to the extensive health metadata available for the Museum of London samples, we focused on this subset. Specifically, we examined overall pathology, blood disorders, nonspecific periostitis, overall vertebral pathology, vertebral facets, Schmorl's nodes, vertebral anomalies, overall joint health, joint osteophytic lipping, joint porosity, abscess, caries, dental hypoplasia, and

periodontitis. Additional data on the recording of these traits can be found in 'A Rapid Method for Recording Human Skeletal Data' by Brian Connell and Peter Rauxloh, a manual available on the Museum of London Website[34].

Dominant genera and associated communities analyses

We initially observed that three key genera drove much of the variation present during PCoA analyes of Bray Curtis distances (Figure 2). We classified these samples into groups using this observation by identified if samples were dominated by either *Actinomyces, Streptococcus*, or *Methanobrevibacter*.

QIIME2

To investigate the dominant community structure in QIIME, we created PCoA plots with biplots (Figures 3A, S5) to understand how species and genera were interrelated with compositional differences. In addition, we used ADONIS to test if the dominant species (i.e., our 'dominant' category, Table S1) was significantly associated with composition, across the all teeth and molar using all taxonomic levels, genera, or species levels and functional subgroups. The dominant species was significantly associated with composition (Table S12).

R Network analysis

To investigate the compositional structure of these groups, we utilized CCLasso (correlation inference for compositional data through Lasso)[35]. We performed CCLasso using both genera and species level data, using individuals dominated by either *Methanobrevibacter,* individuals dominated by *Streptococcus,* and all individuals. We used a correlation threshold of 0.3 and a conservative p-value threshold of 0.0002. We also tested p-value thresholds up to 0.1, and the same results were obtained. No specific numbers of clusters were selected using the igraph R package (https://igraph.org/r/), and we were repeatedly able to visualize two major sets of co-associated taxa across both the genus and species levels. To improve the visualization of the negative correlation results in the text, we limited the number of genera to the most abundant 70 genera. For both visualizations used in the main text, we used the Fruchterman-Reingold layout algorithm for maximal clarity. R code for this analysis is available on Github (@microARCHlab/BritishDentalCalculus_2021).

In addition to visualizing the results using igraph, we also used the inbuild 'heatmap' function in R to visualize a spearman correlation method based on the top 70 most abundant genera (Figure S16). These results demonstrated groupings similar to those observed in the igraph visualizations.

Section 5: Dietary and functional pathway analysis

To determine how diet related to oral microbiome community structures, we used functional pathway analysis. Specifically, we identified functions associated with high and low fiber, carnivory, herbivory, sugars, and lactose (described in Main Text) and explored their presence in the ancient samples (Table S14). For these analyses, complete lists of detected functions were exported from MEGAN6 CE at KEGG (Kyoto Encyclopedia for Genes and Genomes) level 3, SEED level 2, and SEED level 4, as described below. After export from MEGAN using the export text (CSV) format with the seedName_to_count and tab options, the data was introduced to QIIME2 where it was then filtered according to the functions of interest (Table S14). Additionally, only functions with a minimal frequency of 500 sequences were retained.

KEGG Level 3 (fiber metabolism)

Fiber digestion functions associated with high versus low fiber digestion were identified and isolated as previously stated. Samples were then normalized according to the total number of reads in the KEGG Level 3 export in order to generate the heatmap (Figure 4) in excel. In order to formally test whether there were differences in fiber digestion based on the dominant community, the data were also normalized in QIIME2 and tested via ADONIS[36]**.** For both high and low fiber, the ADONIS test returned significant (Pr>F: 0.001) results. Of the 16 of 17 (97.5%) fiber digestion functions identified in the data set (Figure 4, Figure S9), 81% significantly varied across the two community types.

In addition to this test, we also performed Linear discriminant analysis Effect Size (LefSe) tests to determine which functions are most likely to explain the differences between groups[37]. Notably, 70.0% of these functions linked to low-fiber consumption were significantly higher in abundance within the *Streptococcus* groups compare to those dominated by *Methanobrevibacter*, and included galactose metabolism, glycosphingolipid biosynthesis, and glycan degradation (Figure 4, Figure S9).

To corroborate the LefSE results, we also utilized the ALDEx2[38] to identify differentially abundant functions between *Streptococcus* and *Methanobrevibacter* groups for high fiber and low fiber (Table S21; Figure S15E and Figures S15F). Taking both the Expected Benjamini-Hochberg corrected P value of Wilcoxon test and the Expected Benjamini-Hochberg corrected P value of Welch's t-test into account we identified four high-fiber associated functions, as shown in Figure S15E with the associated functions. We also identified nine differentially abundant low-fiber associated functions, as shown in Figure S16F with the associated functions.

SEED Level 2 (carbohydrate metabolism)

Carbohydrate digestion functions were identified and isolated as previously stated. Samples were then normalized according to the total number of reads in the SEED Level 2 export in order to generate the heatmap (Figure 4) in excel. In order to formally test

whether there were differences in carbohydrate digestion based on the dominant community, the data were also normalized in QIIME2 and tested via ADONIS (Anderson 2001). The ADONIS test indicated that the dominant category was significant (R2 = 0.060642, Pr = 0.001).

In addition to this test, we also performed Linear discriminant analysis Effect Size (LefSe) tests to determine which functions are most likely to explain the differences between groups[37]. Of the 124 carbohydrate metabolism associated genes detected in ancient individuals (100%), 46.8% were enriched in *Streptococcus* dominated communities, while only 22.6% were enriched in *Methanobrevibacter* dominated communities, including pathways linked to fructose, sucrose, trehalose, mannose, beta-glucosides, and maltose metabolism (Figure 4; Figure S10). In contrast, *Methanobrevibacter* dominated communities were enriched for functions linked to methanogenesis, gluconeogenesis, and xylose utilization (Figure 4; Figure S10).

Finally, we utilized the ALDEx2[38] to identify differentially abundant functions between *Streptococcus* and *Methanobrevibacter* groups (Table S21; Figure S15D). Taking both the Expected Benjamini-Hochberg corrected P value of Wilcoxon test and the Expected Benjamini-Hochberg corrected P value of Welch's t-test into account, we identified 79 differentially-associated carbohydrate functions.

SEED Level 4 (Herbivory, Carnivory, and Lactose digestion)

Meat and plant consumption were examined by exploring amino acid metabolism functions within the metagenomic diversity since amino acid metabolism pathways are often linked to either carnivore or herbivore diets[39]. Of the 16 functions associated with meat-consumption, 11 (68.75%) were identified within our database. Of the 25 functions associated with plant-consumption, 22 (88.00%) were identified within our database.

First, functions were exported from MEGAN6 CE and filtered as previously stated in order to generate the heatmap (Figure 4) in excel. In order to formally test whether meat and plant consumption differed by dominant community, were performed an ADONIS test and determined that dominant category was significant for meat (R2 = 0.18851, Pr = 0.001) and for plants (R2 = 0.155756, Pr = 0.001).

We also performed Linear discriminant analysis Effect Size (LefSe) tests to determine which functions are most likely to explain the differences between groups[37]. We were able to identify 82.9% (34 of 41) of the amino acid metabolism pathways associated with high or low meat consumption in ancient samples (Table S14), and 88% (30 functions) were significantly more abundant in one of the two groups (Figure 4, Figure S8). While six amino acid functions linked with carnivory were enriched in the *Streptococcus* dominated oral communities (Figure 4, Figure S8), four were increased in abundance in *Methanobrevibacter* dominated communities (Figure 4, Figure S8). Similarly for herbivory, 11 amino acid metabolism functions were linked to *Streptococcus* dominant

communities, while nine were linked to those dominated by *Methanobrevibacter* (Figure 4, Figure S8). Lastly, we verified that the presence of these amino acid metabolism signatures was not linked to periodontal disease, as increases in fatty acid metabolism, acetyl-coenzyme A degradation, aromatic amino acid degradation, ferredoxin oxidation, and energy coupling factor (ECF) class transporters were reported in individuals suffering from periodontal disease (Liu et al. 2012). Only aromatic amino acid aminotransferases were increased in communities dominated by *Streptococcus* species. Together, these findings showed that both oral microbial communities were associated with an omnivorous diet.

The dairy analyses were performed similarly to meat and dairy, with the ADONIS test returning the dominant category as significant ($R2 = 0.367983$, $Pr = 0.001$), and the LefSe analysis indicating that 10 functions were significantly different between the *Methanobrevibacter* and *Streptococcus* associated groups, with most being associated with *Streptococcus* (S11).

We also utilized the ALDEx2[38] to identify differentially abundant functions between *Streptococcus* and *Methanobrevibacter* groups (Table S21; Figures S15A, S15B, S15C). Taking both the Expected Benjamini-Hochberg corrected P value of Wilcoxon test and the Expected Benjamini-Hochberg corrected P value of Welch's t-test into account, we identified 16 functions differentially associated with herbivory, eight differentially associated with carnivory, and 11 differentially associated with lactose. The ALDEx2 analysis were similar to the the LefSE analyses.

Section 6: Bayesian Modeling

In contrast to observations from across all of Great Britain, oral microbiome composition was linked to temporal shifts through time in ancient London ($p < 0.05$; Table 1). While it is possible that temporal effects could be obscured by potentially larger regional variation, showing up only at smaller spatial scales, we first investigated whether the observed temporal effect could be explained by technical variation due to sequence counting[40].

To this end, we fit a Bayesian multinomial logistic-normal linear model[41] to the measurements from ancient London including time as a covariate. This model allowed us to simultaneously infer the proportion of compositional variation that could not be explained sampling noise but could be explained by time. We also defined time as the arrival of the black death (i.e., microbiota prior to 1347, during the Black Death from 1348-1353, and after 1353). Again, we found evidence of substantive temporally-associated compositional variation: 11.16%] of the variability in composition was explained by time (95% credible interval: 5.35% to 18.90%). We next assessed whether this temporally associated variation could be explained by potential confounding due to cemetery-specific effects. We found that 64.83% of the compositional variation explained by time could equally well be explained by cemetery. In short, we found that cemetery could represent a substantial confounding effect, but that cemetery and technical variation alone is unlikely to fully explain the observed temporal trends in microbial composition.

Our results suggest that the composition of oral microbiota in ancient London changed over the 800-year time-period from 1100 to 1900. We found that neither technical variation due to sequence counting nor confounding due to cemetery-specific effects can fully explain the observed temporal trends. Temporal shifts in oral microbiota would be expected throughout history in ancient Britain, given the large-scale shifts in culture, lifestyle, medicine, and hygiene practices that occurred. However, we found that as much as half of temporally associated compositional variation could be explained by cemetery, revealing a key limitation inherent to current approaches for studying ancient microbiomes. It is plausible that previously reported results identify differences in culture or diet could be attributed to these cemetery-based findings, although whether or not cemetery-based shifts in microbiota are linked to biological differences or taphonomic difference remains unknown. Taphonomic bias and inconsistent degradation of remains linked to geography remains a challenging aspect to disentangle from biologically driven spatio-temporal trends. Future work in this area is needed to better investigate signatures of degradation in different areas, especially in the context of biological or cultural trends that shift through time. In particular, we hypothesize that finer resolution of temporal information (e.g., radiocarbon dating of all Museum of London remains) could allow temporal variation within cemeteries to be assessed, potentially quantifying and even controlling for taphonomic verses this spatio-temporal differences.

To identify compositional variation associated with time in ancient London, we first subdivided the full study dataset to samples from the Museum of London that contained temporal information. This resulted in *n = 129* samples. Genera observed with a non-zero count in less than 25% of samples were amalgamated together into a separate category and included in subsequent analyses so as not to lose the variance information contained in the counts[42]. This resulted in 49 genera and a separate category for the amalgamation of filtered genera.

To assess the variability explained by time, we fit a multinomial logistic-normal linear model[41] using the significant temporal Black Death feature as the sole explanatory variable. These methods are efficiently implemented in the *fido* R package[41,42] of which we used version 0.1.13 for our analyses.

Letting Y_{ij} denote the observed abundance for taxa i = 1,...,D in sample j = 1,...N and X denote a Q ×N matrix of covariate information, the general form for these models can be written as:

$$\begin{aligned} Y_j &\sim \ Multinomial\ (\pi_j) \\ \pi_j &= \phi^{-1}(\eta_j) \\ \eta_j &\sim \ N(\Lambda\, X_j, \Sigma) \end{aligned}$$

with priors

$$\begin{aligned} \Lambda &\sim \ MN_{D-1\times Q}(\Theta, \Sigma, \Gamma) \\ \Sigma &\sim IW(\Xi, \nu), \end{aligned}$$

where $\eta_j = \mathrm{ALR}(\pi_j)$ (*e.g.,* η_j denotes the additive log-ratio coordinates of the proportions which exist on the simplex) and $\mathrm{MN}_{D-1\times Q}$ represents the Matrix-Normal distribution of correct dimension[43]. Since linear regression is affine equivariant[44] our model is invariant to the choice of

log-ratio transform provided the prior distributions are correctly re-parametrized. No pseudo counts were used as the Multinomial component of the model handles zeros directly[45].

We fit this model using the previously identified, significant temporal effect as the sole explanatory variable (*i.e.,* an indicator variable for pre/post Black Death), succinctly:

$$\eta \sim N(\Lambda_1 I(Pre - Black\ Death) + \Lambda_2 I(Post - Black\ Death), \Sigma),$$

where I(·) is the usual indicator variable.

Percentage of variation was calculated for each sample using the predicted and actual counts according to the method proposed by Gelman (2019). For priors, $\Theta = \mathbf{0}_{D-1\times Q}$, $\upsilon = D + 3$, $\Xi = G\ I\ G^T$ where $G = [I_{D-1}, -\mathbf{1}_{D-1}]$, and $\Gamma = \gamma\ I_Q$ where γ was tuned using cross-validation to maximize the percentage of explained variation. Under this schema, the Black Death effect explained 11.16% of the variability in the data (95% credible interval: [5.35%, 18.90%]).

To assess the maximal amount of shared variation between time and cemetery, we regressed other covariates of interest onto the fitted values from the previous temporal model (*i.e.*, the variation in composition explained by the previous model). In particular, we focused on cemetery as certain locations were only active during particular time periods. Succinctly, the linear component of our secondary model for the s^{th} sample can be expressed as:

$$\eta^s \sim N(\sum_{i=1}^{9} \Lambda_i\ I(Sample\ from\ Cemetry\ i), \Sigma).$$

Under this schema, cemetery location explained 64.83% of the variability in the data previously explained by the temporal covariate (95% credible interval: [59.84%, 69.00%]).

Due to concerns that these results may be driven by DNA damage, we used a similar specification to study the effect of GC damage on compositional variation. To capture GC damage, we calculated damage profiles for four separate endogenous taxa as determined by MapDamage2.0. Specifically, we used the deltaD (the cytosine deamination probability in double strand context) variable for *Anaerolineaceae bacterium oral taxon 439, Methanobrevibacter oralis, Porphyromonas gingivalis*, and *Streptococcus sanguinis*. We examined this relationship by using the same multinomial logistic-normal linear model specified above using the damage scores for each of the four taxa as explanatory variables. More succinctly, we fit the model specified by:

$$\eta \sim N\left(\Lambda_0 + \sum_{i=1}^{4} \Lambda_i Delta\ D_{taxa\ i}\ , \Sigma\right),$$

For priors, we used a similar specification as before: $\Theta = \mathbf{0}_{D-1\times Q}$, $\upsilon = D + 3$, $\Xi = G\ I\ G^T$ where $G = [I_{D-1}, -\mathbf{1}_{D-1}]$, and $\Gamma = I_Q$. Under this specification, DNA damage across the four selected taxa explained 2.77% of compositional variation (95% credible interval: [1.35%, 4.84%]). Furthermore, we assessed how much variation explained by cemetery is also explained by DNA damage. To do so, we used a similar approach as with the geographic and temporal covariation: we fit an initial model using cemetery location as the sole predictor. Then, we

regressed DNA damage for the four selected taxa on the fitted values from this model. Under this specification, the damage profiles of the four selected taxa explain 1.52% of the compositional variation previously explained by cemetery location (95% credible interval: [0.57%, 3.08%]).

Code for this analysis is available at https://github.com/michellepistner/ancientDNA.

Section 7: Additional Discussion

Oral and Systemic Diseases in Ancient Britain

One of the primary research foci of this study involved how oral and systemic diseases may contribute to microbiome evolution. Well it has been well-established that oral and systemic diseases in modern populations are linked to shifts in plaque microbiota[46], this has not yet been examined in ancient populations. As such, we investigated the associations of 14 different indicators of oral and systemic health on ancient London oral microbiotas. While no associations between oral microbiota in all teeth and oral or systemic disease were observed, this was not the case when examining only molar teeth, highlighting the importance of accounting for tooth type in ancient calculus data sets.

For oral diseases, all taxa in molars were associated with the presence of periodontal disease ($R2 > 0.05$; $p < 0.05$; Table 1), but not the presence of caries, abscesses, or hypoplasia. For skeletal markers of systemic disease, overall microbiota composition was linked to several systemic disease markers, including nonspecific periostitis, osteophytic lipping, and joint porosity, as well as general scores for overall pathologies or joint deterioration ($R2 > 0.05$; $p < 0.05$; Table 1). Non-specific periostitis was linked to species identified the *Methanobrevibacter* dominated community, including *Methanobrevibacter*, *Eubacterium*, *Pseudoramibacter*, *Mogibacterium*, and *Petoniphilus* species (Table S19). The presence of nonspecific periostitis is thought to be linked to the inflammation of tissue surrounding the bone[47–49] and its association with various diseases (including syphilis and skin ulcers) and is linked with trauma[47]. Similarly, osteophytic lipping and porosity were also linked to key species present within the *Methanobrevibacter* community, suggesting that systemic inflammation may be linked to the presence of the *Methanobrevibacter* dominated oral microbial community. These signatures in skeletal stress have also been previously linked to individuals of lower socioeconomic status in the past[6], highlighting the need to examine how diet, socioeconomic status, and disease work together to shape microbiota. Together, these results highlight associations between oral microbiota and systemic disease, and although cause and effect remain unclear, this suggests that reconstructing ancient oral microbiota may provide insights into invisible or non-communicable diseases within the archaeological record. Our results suggest that the composition of oral microbiota in ancient London changed over the 800-year time-period from 1100 to 1900.

This is a key finding for the field, as recent temporal trends were not observed using alternative methods[50], although that approach could have been confounded by the

sampling strategy (i.e., failing to sample a consistent tooth type and amalgamating samples across multiple teeth) and lack of considerations for confounding factors.

Socioeconomic Status and the Oral Microbiome

Socio-economic rank has been associated with differential access to food items throughout history. The *Streptococcus* dominated microbiota samples contain metabolic functions linked to meat, low-fiber carbohydrate, and dairy consumption. This is in stark contrast to the *Methanobrevibacter* dominated communities, which was linked to a high-fiber, plant-based diet. These observations may be linked with diets that are related to different lifestyles or socioeconomic ranks. For example, lower classes in Britain during the period analyzed had a diet dominated by cereals and vegetables, while wealthier individuals (aristocracy, upper clergy, and wealthy townspeople) had additional access to meat and fish[51]. Further, bone diseases linked to greater physical stress and malnutrition are typically seen in ancient individuals with low socio-economic rank[52]. In London, low socioeconomic status has been previously associated with poor bone health[52]. While it is possible that these bone diseases directly led to alterations in microbiota, it is also possible that these relationships between disease and microbiota are explained by greater lifestyle factors, such as low socioeconomic status. In fact, several studies to date have linked socioeconomic status to microbiota community composition[53–55]. While we do not have the ability to estimate socioeconomic status from these individuals using archaeological signatures, our results are consistent with observations of socioeconomic status and may suggest that oral microbiota can be used as a marker for socioeconomic status in the past. Further research is needed to investigate this trend in different human cultures, both locally and globally.

Impacts of the Plague Pandemic on the Oral Microbiome

The arrival of *Y. pestis* in Britain resulted in the deaths of over 30-50% of Londoners between 1348 to 1351 alone[56], changing the social, economic, and cultural lives of the survivors. These substantial changes both directly and indirectly impacted the health, and potentially the microbiomes, of the survivors. From a direct biological perspective, the plague was selective with respect to more frail individuals[57]. That frailty may have been caused by malnutrition, immunocompetence, or other factors whose rates in the general population would have shifted after the disease had passed. In addition to biological selection, other significant factors shifted during this period that would have influenced health. For example, there was less warfare and a decreased price of goods, thereby impacting lifestyles[58]. The changing social climate also led to the alteration of diets as the proportion of agricultural land to pastures decreased, thereby leading to an increase in meat and other animal product consumption, as supported by both historic and biological (isotopic) evidence[59]. These factors (disease selection, changing social climates, shifting diets) could have had substantial impacts on the health and microbial-ecosystems of surviving populations.

It is prudent to note that there is some level of disagreement regarding the selective pressures associated with the pandemic, and that more work therefore needs to be done on these topics[60,61], particularly with respect to how they may directly or indirectly lead to microbiome changes. With respect to the demographic impact of the pandemic, there are also mixed perspectives and results about how the pandemic may have impacted genetic diversity in different areas[62,63]. As such, while our results do indicate a temporal trend that fits with the timeline of the pandemic, more research needs to be conducted to discern the specific mechanisms leading to these changes and delineating the impacts of the pandemic itself versus changes that occurred in the decades and centuries that followed (shifting migration patterns, industrialization, etc.).

Limitations associated with sub versus supra-gingival samples

One challenge of this study is that classifying supra- verses subgingival dental calculus is not straight forward in archaeological contexts, as the ability to macroscopically identify supra- and sub- gingival calculus in the context of the gingival margin in past population may be less clear[6]. For example, Hill described supragingival calculus as "clay-like deposits that in life run along the edge of the gums or gingivae, [Supragingival calculus] may be on the crown only, or extend onto the roots when they were exposed above the gums"[64]. This description clearly fits the description of all supragingival dental calculus collected in this study, but are also clearly at odds with calculus collected by other teams[65]. However, the results shown here raise questions about the binary delineation of sub and supragingival dental calculus in archaeological contexts. As calculus can form over the lifetime of an individual, it is possible that delineated supra- and subgingival deposits become overlapping, as tooth eruption or bone loss progresses. More work is needed to clarify microbial associations between supra- and subgingival calculus as it exists in the archaeological record, and improved tools to describe the differences in archaeological calculus will undoubtedly result in an improved understanding about past oral health and the formation of dental calculus more broadly[66].

Limitations associated with DNA fragment length of dominant communities

As shown in Figure S19, the *Methanobrevibacter* and *Streptococcus*-associated samples exhibited statistically significant distributions of assigned sequences ($t = -4.9244$, $df = 60.609$, p-value = 6.85e-06). While more research is required to fully understand these differential patterns, we hypothesize that the reason for this may be due to the differences in GC content and cell wall structure of the dominant genus[67]. For example, Methanobrevibacter genomes have much lower GC content than *Streptococcus* species, which impacts the recovery of their DNA[68]. We would therefore expect the read lengths of *Methanobrevibacter*-dominated communities to have shorter DNA fragments, as observed, but the impacts of DNA fragment length on community recovery and assessment need further research.

Conclusions

The presence of *Methanobrevibacter* species, such as *M. oralis*, in people living in Industrialized countries today are linked to subgingival dental calculus in individuals suffering from periodontal disease[69,70]; for example, *M. oralis* has been described in the subgingival crevice of people suffering from periodontal disease[70]. Methanobrevibacter has also been identified in modern smokers[71]. In ancient peoples, *M. oralis* has also been found in supragingival calculus in both Neandertals and anatomically modern humans without signs of periodontal disease (as defined by bone loss), pointing to a broader presence in past humans[69,72]. This is also supported by the lack of detection of *Methanobrevibacter* in oral microbiome studies of modern individuals[73], suggesting that *Methanobrevibacter*-associated communities are less likely to be found in modern populations. In contrast, methanogens have been identified in nearly every ancient calculus microbiome study published to date across Europe and Asia (e.g., [2,4,21,68,72]), suggesting that this genus and its associated species were common in the calculus of past individuals.

Consequently, our data is consistent with major changes in oral microbiota occurring during and following the Industrial Revolution. The Industrial Revolution saw marked increases in sugar consumption, notably sucrose and fructose. Processing of cereal grains became capable of removing germ and bran from the milled flour, reducing the fiber content. Consumption of dairy products and fatty meats also grew[74]. Further changes after the Industrial Revolution, such as tooth brushing and exposure to antibiotics[75], may have also further shifted ancient microbiota toward that observed today. While the effect of antibiotics on the oral microbiome is thought to be minimal[76], it may have shifted the oral microbiome over a significant time span. However, this does not rule out the possibility that these microbiotas still exist in people with large amounts of dental calculus or in other contexts, especially other microecologies where large anaerobic pockets in the mouth exist. Nevertheless, the Industrial Revolution likely provided a refined version of the *Streptococcus* dominated communities, which spread to the whole population. Given the functional characteristics linked to diet, we hypothesize that *Streptococcus*-associated microbiota became dominant once a high-status diet was widely adopted in modern, Industrialized societies.

Our study suggests that there are limitations to these approaches and that ancient dental calculus studies should work toward more ethical, sustainable sampling practices and should account for oral geography when examining correlations between individual metadata and oral microbiota. Even though it markedly reduced the total sample size per group, intrapersonal variation largely masked many of the links between disease and microbiota. Notably, different sampling locations within the mouth also revealed individual associations with skeletal metadata. While limited sample numbers in some tooth groupings may affect these findings, oral microbial communities from different teeth may also respond differently in states of disease, providing additional sources of information to understand the microbial biology that underpins disease. These results are in stark contrast to published research that suggesting that the impacts of oral geography

are minor[31]; these conclusions were likely reached by inferring population level effects from four individuals in a single population. The impact of oral geography may also differ according to whether or not a single population or multiple, distinct populations are being examined.

Section 8: Data Deposition

All trimmed and merged DNA sequences (fastq) are available on SRA databases (BioProject PRJNA780005). The individual metadata and analysis methods are available on the microARCH's github page (@microARCHlab/BritishDentalCalculus_2021). Unmerged reads may be made available upon request.

Section 9: Supplementary References

1. Wellcome Osteological database. *Museum of London* https://www.museumoflondon.org.uk/collections/other-collection-databases-and-libraries/centre-human-bioarchaeology/osteological-database (2021).
2. Weyrich, L. S. *et al.* Neanderthal behaviour, diet, and disease inferred from ancient DNA in dental calculus. *Nature* **544**, 357–361 (2017).
3. Belda-Ferre, P. *et al.* The oral metagenome in health and disease. *ISME J* **6**, 46–56 (2012).
4. Warinner, C. *et al.* Pathogens and host immunity in the ancient human oral cavity. *Nat. Genet.* **46**, 336–344 (2014).
5. McMurdie, P. J. & Holmes, S. Waste Not, Want Not: Why Rarefying Microbiome Data Is Inadmissible. *PLOS Computational Biology* **10**, e1003531 (2014).
6. Warinner, C., Speller, C., Collins, M. J. & Lewis, C. M. Ancient human microbiomes. *J Hum Evol* **0**, 125–136 (2015).
7. Radini, A., Nikita, E., Buckley, S., Copeland, L. & Hardy, K. Beyond food: The multiple pathways for inclusion of materials into ancient dental calculus. *American Journal of Physical Anthropology* **162**, 71–83 (2017).
8. Weyrich, L. S., Dobney, K. & Cooper, A. Ancient DNA analysis of dental calculus. *J. Hum. Evol.* **79**, 119–124 (2015).
9. Adler, C. J. *et al.* Sequencing ancient calcified dental plaque shows changes in oral microbiota with dietary shifts of the Neolithic and Industrial revolutions. *Nat Genet* **45**, 450–455 (2013).
10. Farrer, A. G. *et al.* Effectiveness of decontamination protocols when analyzing ancient DNA preserved in dental calculus. *Sci Rep* **11**, 7456 (2021).
11. Brotherton, P. *et al.* Neolithic mitochondrial haplogroup H genomes and the genetic origins of Europeans. *Nature Communications* **4**, 1764 (2013).
12. najoshi. najoshi/sabre. (2021).

13. Lindgreen, S. AdapterRemoval: easy cleaning of next-generation sequencing reads. *BMC Research Notes* **5**, 337 (2012).
14. Herbig, A. *et al.* MALT: Fast alignment and analysis of metagenomic DNA sequence data applied to the Tyrolean Iceman. *bioRxiv* 050559 (2016) doi:10.1101/050559.
15. Eisenhofer, R. & Weyrich, L. S. Proper Authentication of Ancient DNA Is Still Essential. *Genes (Basel)* **9**, (2018).
16. Hillmann, B. *et al.* Evaluating the Information Content of Shallow Shotgun Metagenomics. *mSystems* **3**, e00069-18 (2018).
17. Moore, N. E. & Weyrich, L. S. A Standardized Approach for Shotgun MetagenomicMetagenomicsAnalysis of Ancient Dental CalculusDental calculusMetagenomics. in *The Oral Microbiome: Methods and Protocols* (ed. Adami, G. R.) 93–118 (Springer US, 2021). doi:10.1007/978-1-0716-1518-8_7.
18. Davis, N. M., Proctor, D. M., Holmes, S. P., Relman, D. A. & Callahan, B. J. Simple statistical identification and removal of contaminant sequences in marker-gene and metagenomics data. *Microbiome* **6**, 226 (2018).
19. Escapa, I. F. *et al.* New Insights into Human Nostril Microbiome from the Expanded Human Oral Microbiome Database (eHOMD): a Resource for the Microbiome of the Human Aerodigestive Tract. *mSystems* **3**, e00187-18 (2018).
20. Knights, D. *et al.* Bayesian community-wide culture-independent microbial source tracking. *Nat Methods* **8**, 761–763 (2011).
21. Velsko, I. M. *et al.* Microbial differences between dental plaque and historic dental calculus are related to oral biofilm maturation stage. *Microbiome* **7**, 102 (2019).
22. Eisenhofer, R., Kanzawa-Kiriyama, H., Shinoda, K. & Weyrich, L. S. Investigating the demographic history of Japan using ancient oral microbiota. *Philos Trans R Soc Lond B Biol Sci* **375**, 20190578 (2020).

23. Velsko, I. M. *et al.* The dental calculus metabolome in modern and historic samples. *Metabolomics* **13**, 134 (2017).
24. Califf, K. J. *et al.* Multi-omics Analysis of Periodontal Pocket Microbial Communities Pre- and Posttreatment. *mSystems* **2**, e00016-17 (2017).
25. Pérez, V., Liu, Y., Hengst, M. B. & Weyrich, L. S. A Case Study for the Recovery of Authentic Microbial Ancient DNA from Soil Samples. *Microorganisms* **10**, 1623 (2022).
26. Larson, P. J. *et al.* Associations of the skin, oral and gut microbiome with aging, frailty and infection risk reservoirs in older adults. *Nat Aging* **2**, 941–955 (2022).
27. Liu, Y. The Role of Epigenetic Modications and Microbiome Evolution in Bovid Adaptation to Environmental Changes. (2019).
28. Jónsson, H., Ginolhac, A., Schubert, M., Johnson, P. L. F. & Orlando, L. mapDamage2.0: fast approximate Bayesian estimates of ancient DNA damage parameters. *Bioinformatics* **29**, 1682–1684 (2013).
29. Simón-Soro, A. & Mira, A. Solving the etiology of dental caries. *Trends Microbiol* **23**, 76–82 (2015).
30. Farrer, A. G. *et al.* Biological and cultural drivers of oral microbiota in Medieval and Post-Medieval London, UK | bioRxiv. (2018).
31. Fagernäs, Z. *et al.* Understanding the microbial biogeography of ancient human dentitions to guide study design and interpretation. *FEMS Microbes* **3**, xtac006 (2022).
32. McDonald, D. *et al.* American Gut: an Open Platform for Citizen Science Microbiome Research. *mSystems* **3**, e00031-18 (2018).
33. White, D. J. Dental calculus: recent insights into occurrence, formation, prevention, removal and oral health effects of supragingival and subgingival deposits. *Eur J Oral Sci* **105**, 508–522 (1997).
34. Connell, B. & Rauxloh, P. *A rapid method for recording human skeletal data.* (2003).
35. Fang, H., Huang, C., Zhao, H. & Deng, M. CCLasso: correlation inference for compositional data through Lasso. *Bioinformatics* **31**, 3172–3180 (2015).

36. Anderson, M. J. A new method for non-parametric multivariate analysis of variance. *Austral Ecology* **26**, 32–46 (2001).
37. Segata, N. *et al.* Metagenomic biomarker discovery and explanation. *Genome Biol* **12**, R60 (2011).
38. Fernandes, A. D., Macklaim, J. M., Linn, T. G., Reid, G. & Gloor, G. B. ANOVA-like differential expression (ALDEx) analysis for mixed population RNA-Seq. *PLoS One* **8**, e67019 (2013).
39. Muegge, B. D. *et al.* Diet drives convergence in gut microbiome functions across mammalian phylogeny and within humans. *Science* **332**, 970–974 (2011).
40. Gloor, G. B., Macklaim, J. M., Vu, M. & Fernandes, A. D. Compositional uncertainty should not be ignored in high-throughput sequencing data analysis. *Austrian Journal of Statistics* **45**, 73–87 (2016).
41. Silverman, J. D., Roche, K., Holmes, Z. C., David, L. A. & Mukherjee, S. Bayesian Multinomial Logistic Normal Models through Marginally Latent Matrix-T Processes. *arXiv:1903.11695 [stat]* (2019).
42. Silverman, J. fido (formerly stray). (2021).
43. Gupta, A. K. & Nagar, D. K. *Matrix variate distributions*. (Chapman & Hall, 2000).
44. Eaton, M. L. *Multivariate Statistics: A Vector Space Approach*. (John Wiley & Sons Inc, 1983).
45. Silverman, J. D., Roche, K., Mukherjee, S. & David, L. A. *Naught all zeros in sequence count data are the same*. 477794 https://www.biorxiv.org/content/10.1101/477794v1 (2018) doi:10.1101/477794.
46. Shaw, L. P., Smith, A. M. & Roberts, A. P. The oral microbiome. *Emerg Top Life Sci* **1**, 287–296 (2017).
47. Ortner, D. J. *Identification of Pathological Conditions in Human Skeletal Remains*. (Academic Press, 2003).
48. Weston, D. A. Investigating the specificity of periosteal reactions in pathology museum specimens. *Am J Phys Anthropol* **137**, 48–59 (2008).

49. Weston, D. A. Nonspecific Infection in Paleopathology: Interpreting Periosteal Reactions. in *A Companion to Paleopathology* 492–512 (John Wiley & Sons, Ltd, 2011). doi:10.1002/9781444345940.ch27.
50. Fellows Yates, J. A. *et al.* The evolution and changing ecology of the African hominid oral microbiome. *Proceedings of the National Academy of Sciences* **118**, e2021655118 (2021).
51. Müldner, G. & Richards, M. P. Fast or feast: reconstructing diet in later medieval England by stable isotope analysis. *Journal of Archaeological Science* **32**, 39–48 (2005).
52. Newman, S. L. & Gowland, R. L. Dedicated Followers of Fashion? Bioarchaeological Perspectives on Socio-Economic Status, Inequality, and Health in Urban Children from the Industrial Revolution (18th–19th C), England. *International Journal of Osteoarchaeology* **27**, 217–229 (2017).
53. Miller, G. E. *et al.* Lower Neighborhood Socioeconomic Status Associated with Reduced Diversity of the Colonic Microbiota in Healthy Adults. *PLOS ONE* **11**, e0148952 (2016).
54. Belstrøm, D. *et al.* Bacterial profiles of saliva in relation to diet, lifestyle factors, and socioeconomic status. *J Oral Microbiol* **6**, (2014).
55. Mason, M. R., Nagaraja, H. N., Camerlengo, T., Joshi, V. & Kumar, P. S. Deep Sequencing Identifies Ethnicity-Specific Bacterial Signatures in the Oral Microbiome. *PLOS ONE* **8**, e77287 (2013).
56. Shrewsbury, J. F. D. *A History of Bubonic Plague in the British Isles*. (Cambridge University Press, 2005).
57. DeWitte, S. N. & Wood, J. W. Selectivity of Black Death mortality with respect to preexisting health. *Proceedings of the National Academy of Sciences* **105**, 1436–1441 (2008).
58. Bridbury, A. R. The Black Death. *The Economic History Review* **26**, 577–592 (1973).
59. Zechini, M. E., Killgrove, K., Melisch, C. M., Turner, B. L. & Schaefer, B. J. Diachronic changes in diet in medieval Berlin: Comparison of dietary isotopes from pre- and post-Black Death adults. *Journal of Archaeological Science: Reports* **38**, 103064 (2021).

60. Klunk, J. *et al.* Evolution of immune genes is associated with the Black Death. *Nature* **611**, 312–319 (2022).

61. Barton, A. R. *et al.* Insufficient evidence for natural selection associated with the Black Death. 2023.03.14.532615 Preprint at https://doi.org/10.1101/2023.03.14.532615 (2023).

62. Gopalakrishnan, S. *et al.* The population genomic legacy of the second plague pandemic. *Current Biology* **32**, 4743-4751.e6 (2022).

63. Klunk, J. *et al.* Genetic resiliency and the Black Death: No apparent loss of mitogenomic diversity due to the Black Death in medieval London and Denmark. *American Journal of Physical Anthropology* **169**, 240–252 (2019).

64. Hillson, S. Dental Anthropology. *Cambridge Core* https://www-cambridge-org.ezaccess.libraries.psu.edu/core/books/dental-anthropology/5AE1FF83354B4C33BEDCE0327558B97F (1996) doi:10.1017/CBO9781139170697.

65. Mann, A. E. *et al.* Differential preservation of endogenous human and microbial DNA in dental calculus and dentin. *Scientific Reports* **8**, 1–15 (2018).

66. Greene, T. R., Kuba, C. L. & Irish, J. D. Quantifying calculus: A suggested new approach for recording an important indicator of diet and dental health. *HOMO* **56**, 119–132 (2005).

67. Arning, N. & Wilson, D. J. The past, present and future of ancient bacterial DNA. *Microb Genom* **6**, mgen000384 (2020).

68. Ziesemer, K. A. *et al.* Intrinsic challenges in ancient microbiome reconstruction using 16S rRNA gene amplification. *Sci Rep* **5**, 16498 (2015).

69. Horz, H.-P. & Conrads, G. Methanogenic Archaea and oral infections — ways to unravel the black box. *J Oral Microbiol* **3**, 10.3402/jom.v3i0.5940 (2011).

70. Lepp, P. W. *et al.* Methanogenic Archaea and human periodontal disease. *PNAS* **101**, 6176–6181 (2004).

71. Grine, G. *et al.* Tobacco-smoking-related prevalence of methanogens in the oral fluid microbiota. *Sci Rep* **8**, 9197 (2018).

72. Granehäll, L. *et al.* Metagenomic analysis of ancient dental calculus reveals unexplored diversity of oral archaeal Methanobrevibacter. *Microbiome* **9**, 197 (2021).
73. Handsley-Davis, M. *et al.* Heritage-specific oral microbiota in Indigenous Australian dental calculus. *Evolution, Medicine, and Public Health* **10**, 352–362 (2022).
74. Cordain, L. *et al.* Origins and evolution of the Western diet: health implications for the 21st century. *Am J Clin Nutr* **81**, 341–354 (2005).
75. Weyrich, L. S. The evolutionary history of the human oral microbiota and its implications for modern health. *Periodontology 2000* **85**, 90–100 (2021).
76. Zaura, E. *et al.* Same Exposure but Two Radically Different Responses to Antibiotics: Resilience of the Salivary Microbiome versus Long-Term Microbial Shifts in Feces. *mBio* **6**, e01693-01615 (2015).

Figure S1: PCoA (Bray Curtis) at the Genus Level of British, MoL, and EBC Samples

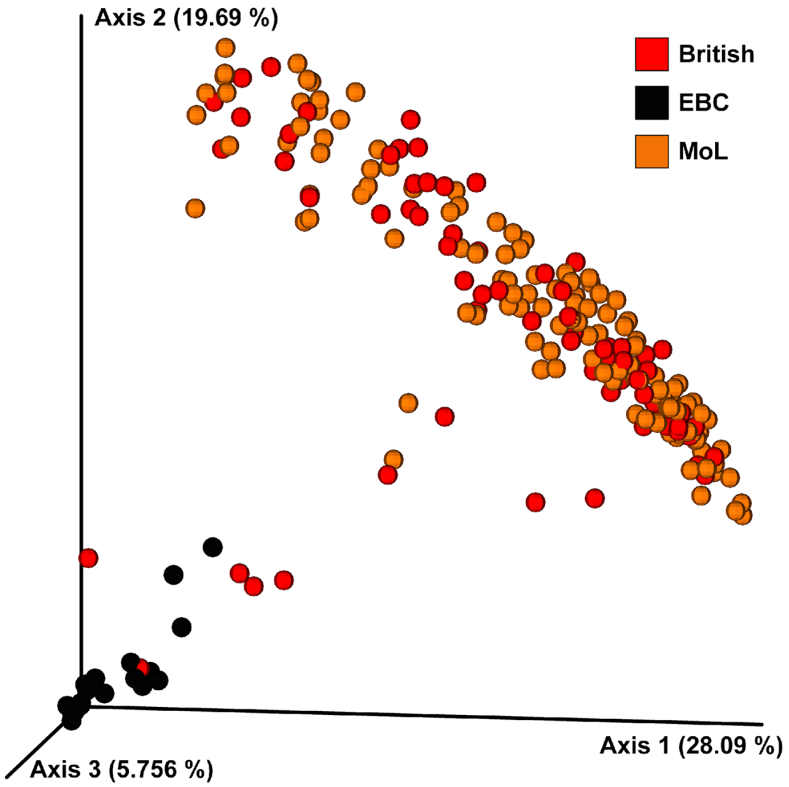

Figure S1: A Principal Coordinates of Analysis (PCoA) plot displaying differences in Bray Curtis distances in microbial genera within the British, Museum of London (MoL), and extraction blank control (EBC) samples.

Figure S2: MALTx SourceTracker Analysis

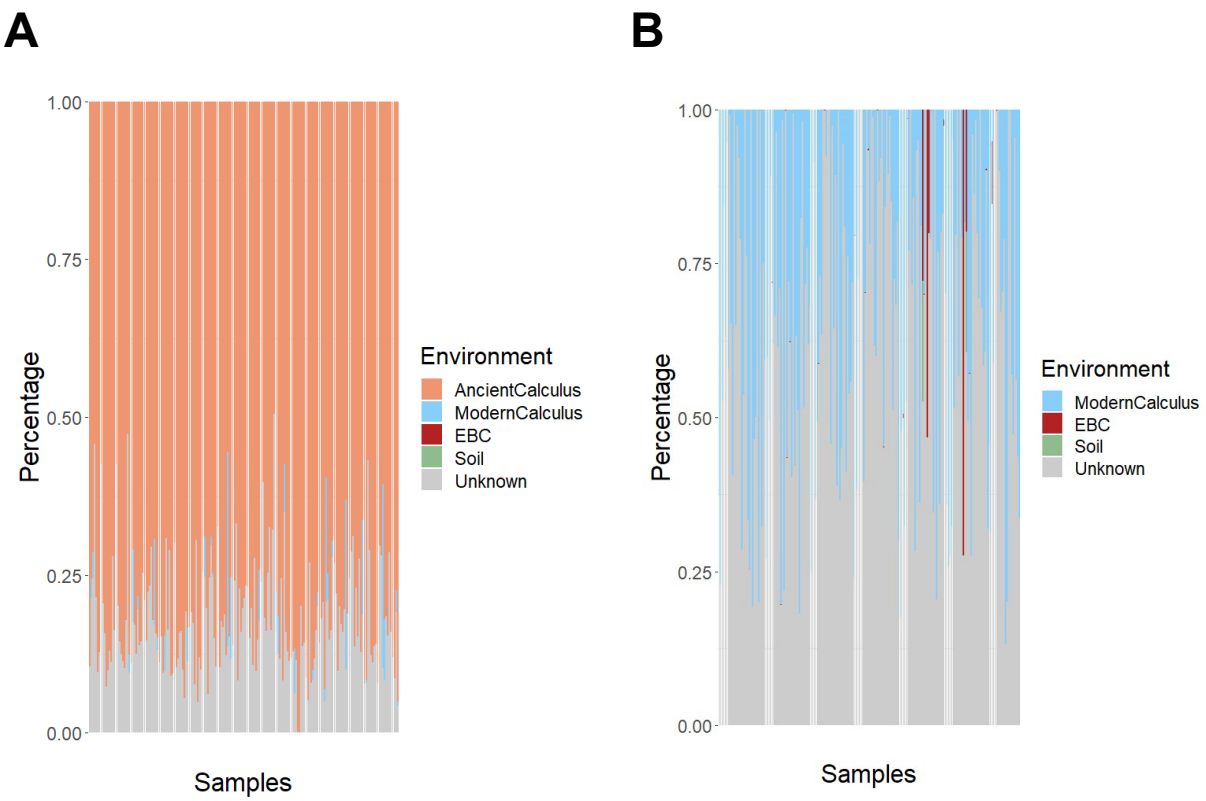

Figure S2: A SourceTracker analysis of the ancient British samples as compared to extraction blank controls (EBCs), modern human calculus, and soil. Panel (A) displays the analysis with ancient calculus references included, and panel (B) only includes modern calculus, EBCs, soil, and unknown sources.

Figure S3: Sample aDNA Authentication Workflow

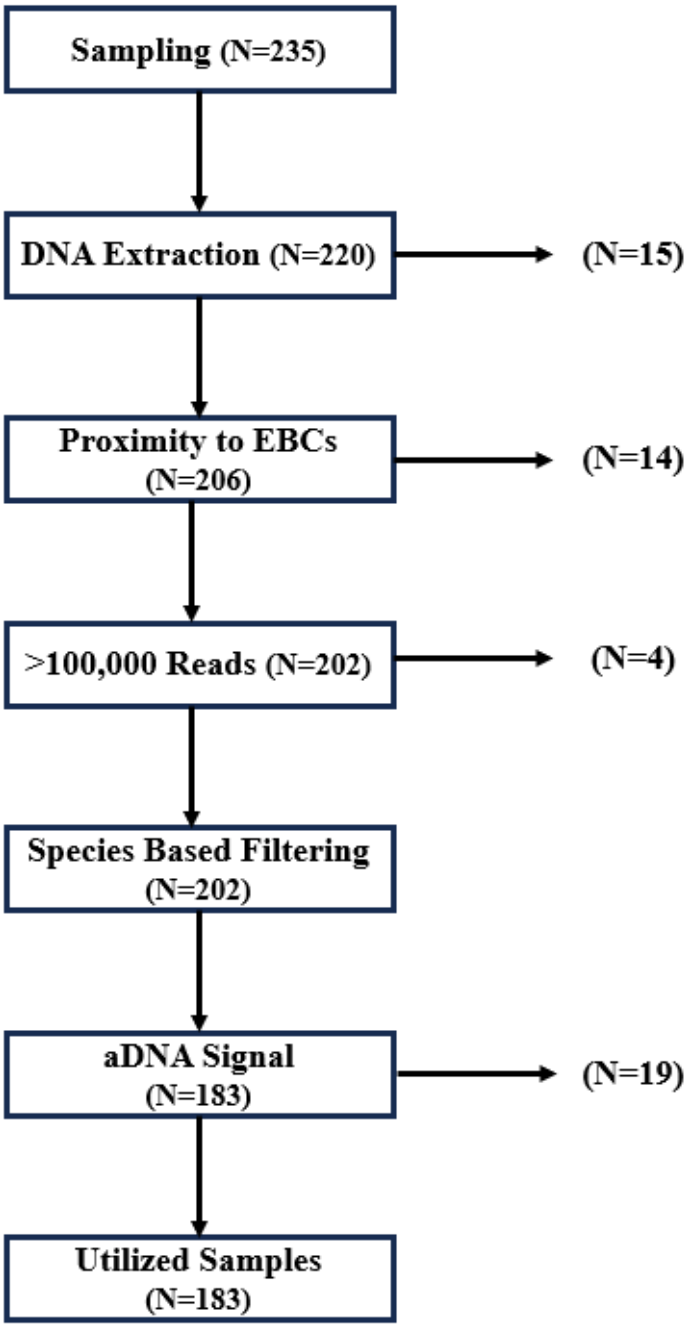

Figure S3: Ancient DNA and Authentication workflow for this study including the relevant steps and the numbers of samples retained and discarded at each. The procedures were conducted left to right in order. Following sampling, 15 samples were discarded due to a lack of DNA recovery after DNA extraction. 14 samples were compositionally similar to the extraction blank controls (EBCs) and were therefore discarded (see SI text for details). Another four samples had fewer than 100,000 assigned reads and were therefore discarded to accurately reconstruct diversity. For species-based analyses, we also filtered out species found in the EBCs. Finally, we used MapDamage2.0 and ChangePoint to determine whether samples had DNA-damage patterns as expected in ancient samples; samples without meaningful DNA damage were excluded from downstream analyses.

Figure S4: Barplots at the Phylum, Genus, and Species Levels

A

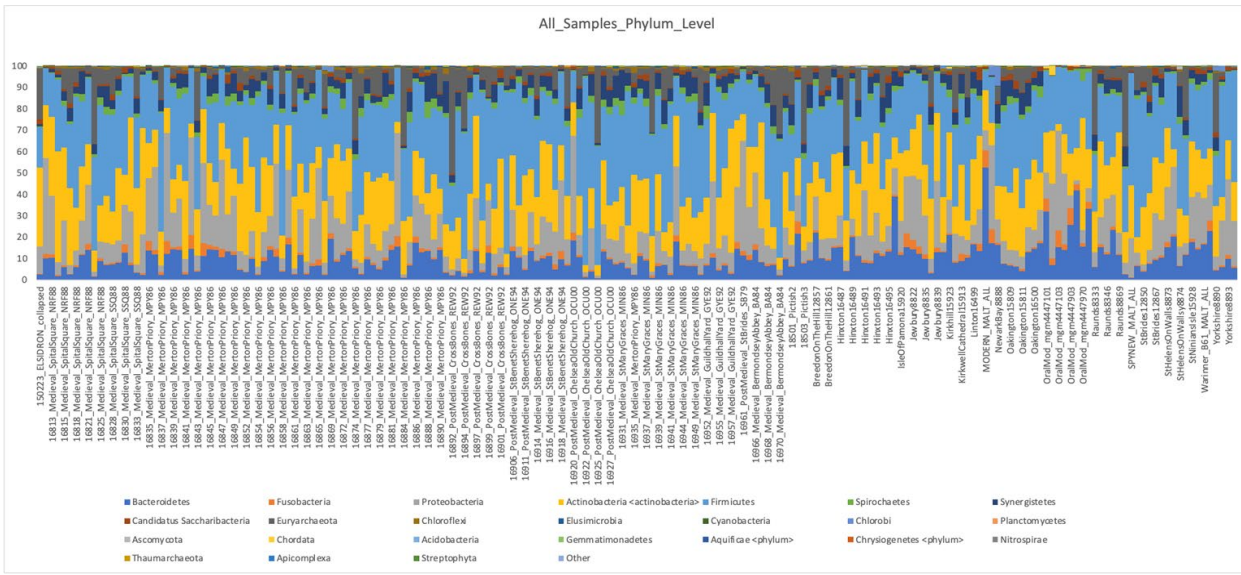

B

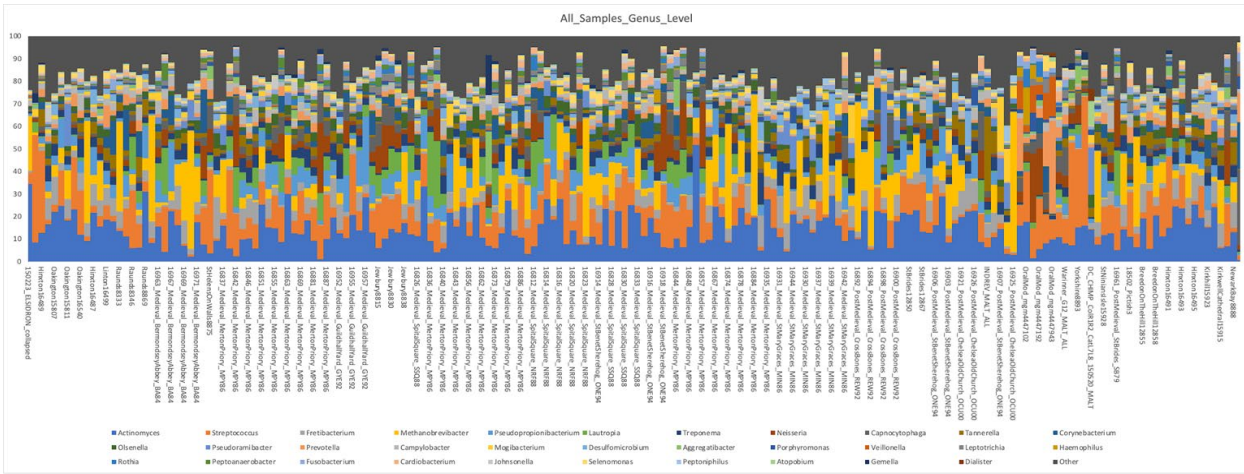

C

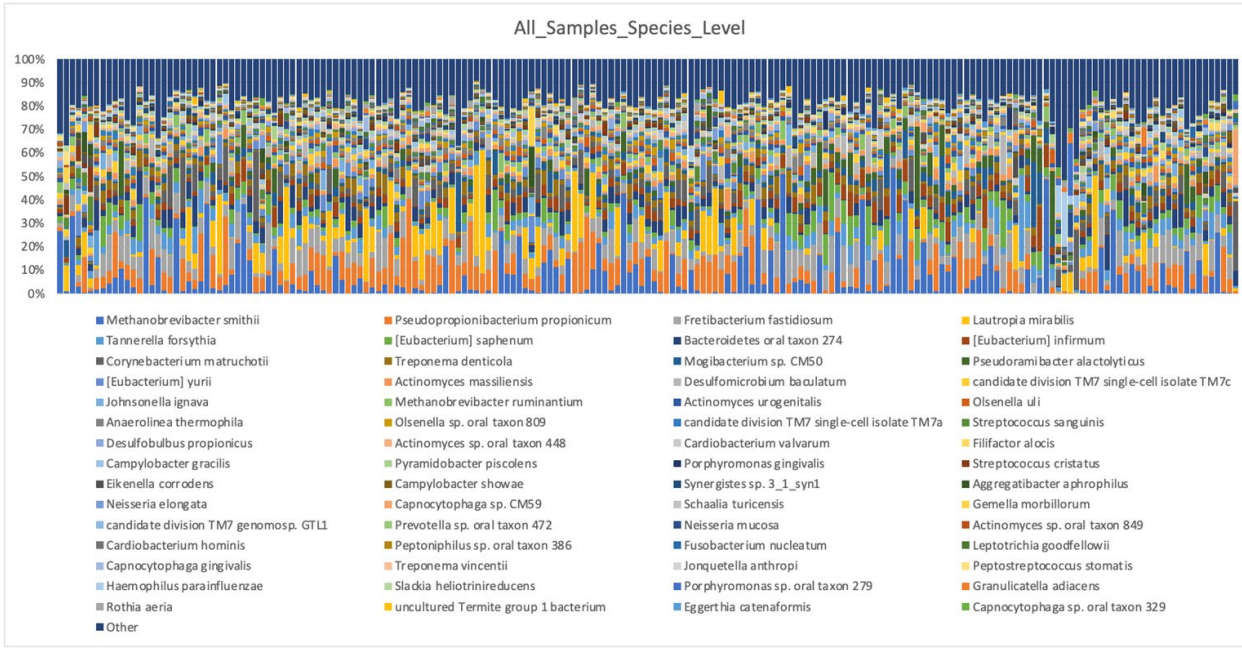

Figure S4: Barplots at the Phylum, Genus, and Species Levels

D

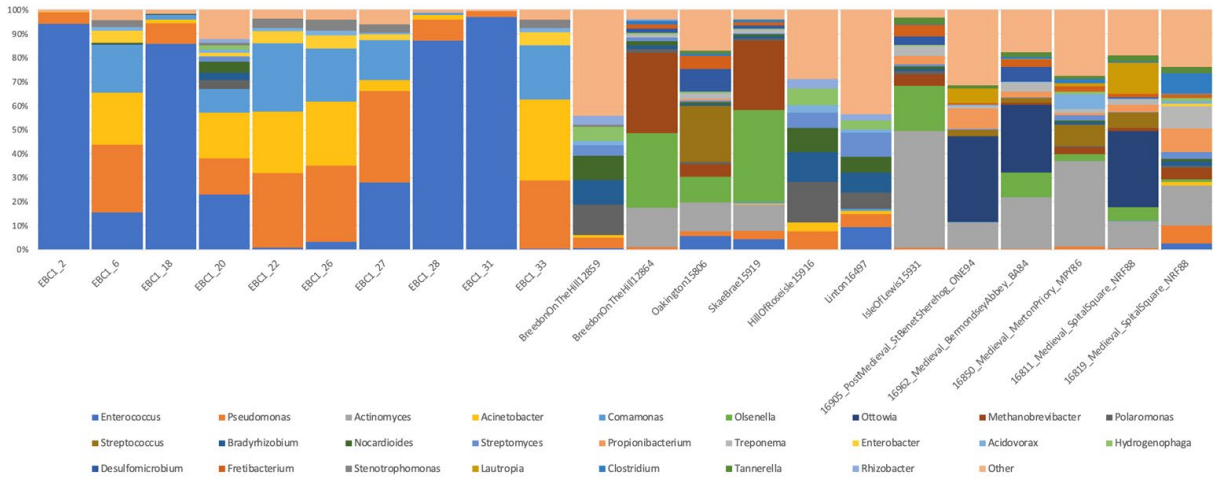

Figure S4: (A) A stacked barplot at the phylum level showing the top 24 phyla within the samples included in this study. (B) A stacked barplot at the genera level showing the top 32 genera within the samples included in this study. (C) A stacked barplot at the species level showing the top 60 species within the samples included in this study. (D) The top 25 taxa found in EBCs and failed samples (i.e., those with non-significant amounts of DNA damage via ChangePoint analysis) are shown in a stacked bar plot.

Figure S5: PCoA of Dominant Taxa

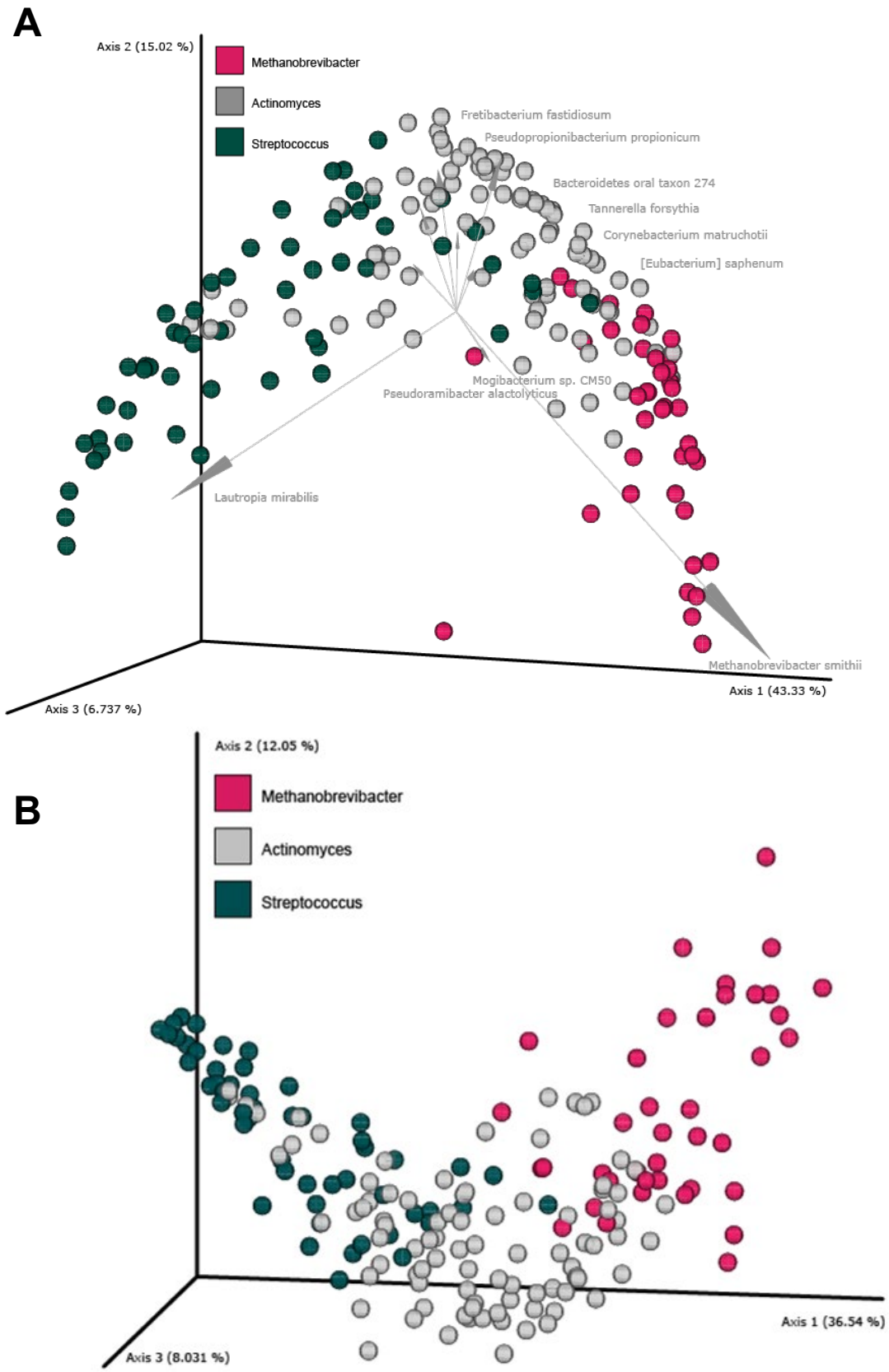

Figure S5: A Principal Coordinates of Analysis (PCoA) plot of Bray Curtis distances of taxa at the species level (A) or functional gene families exported at level 4 (B) showing the distribution of *Methanobrevibacter* (pink) and *Streptococcus* (green) dominated samples. The top-ten species calculated using Biplots are also shown in A.

Figure S6: PCoA of Ancient and Modern Taxa and ADONIS Results

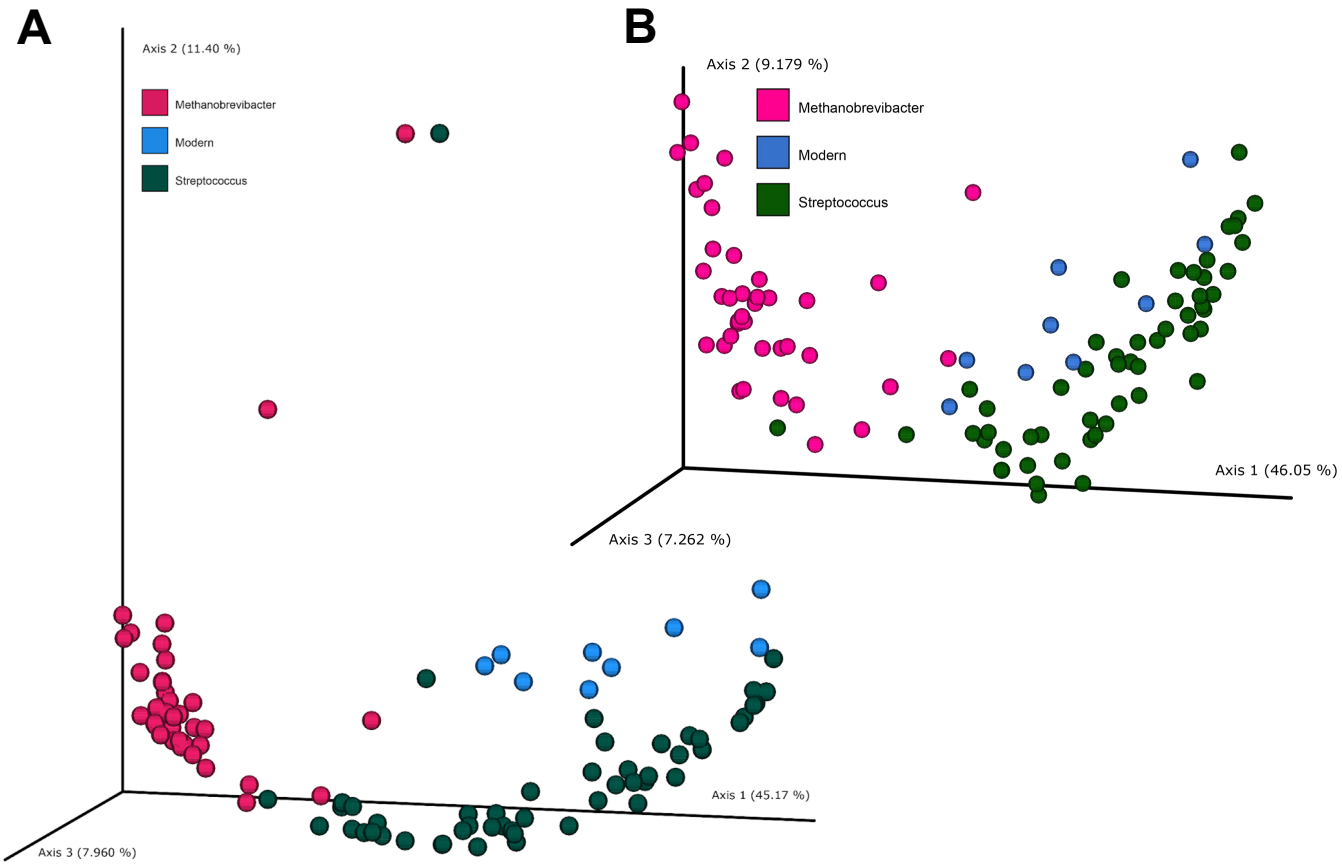

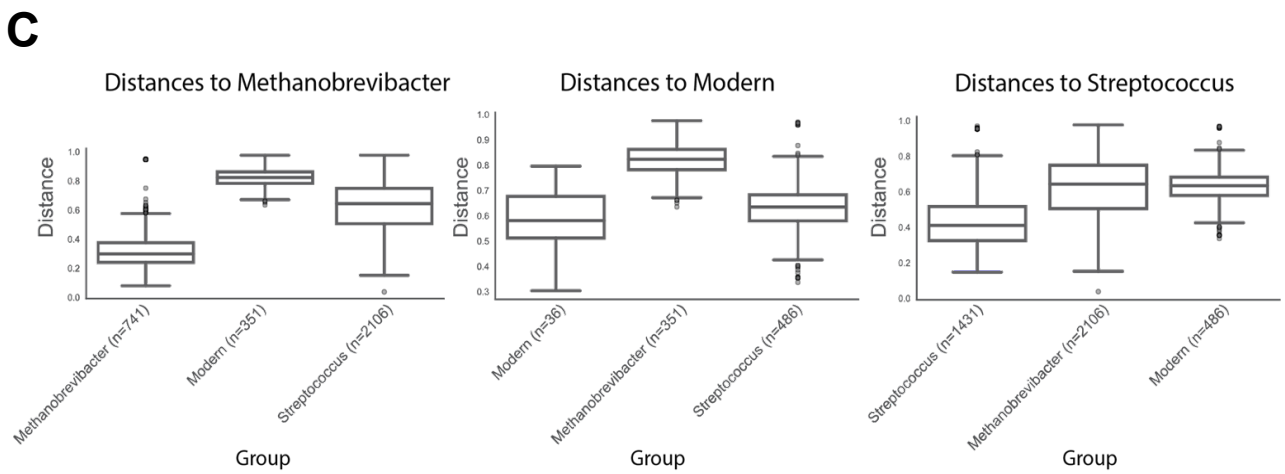

Figure S6: (A) A Principal Coordinates of Analysis (PCoA) plot of Bray Curtis distances at the species level demonstrating the distribution of *Methanobrevibacter* (pink), *Streptococcus* (green), and modern (blue) samples. This was done to further explore which community may be more similar to that in modern, Industrialized peoples. (B) A Principal Coordinates of Analysis plot of the Bray Curtis distances at the genus level with the same color coding as A. (C) The group significance results comparing the three groups at the all taxa level are displayed, with boxplots showing the minimum, 25th, 50th, and 75th, and maximum percentiles (excluding outliers) respectively (Modern = 9, Streptococcus =54, Methanobrevibacter = 39).

Figure S7: Genus-Level PCoAs Based on Region and Time Periods

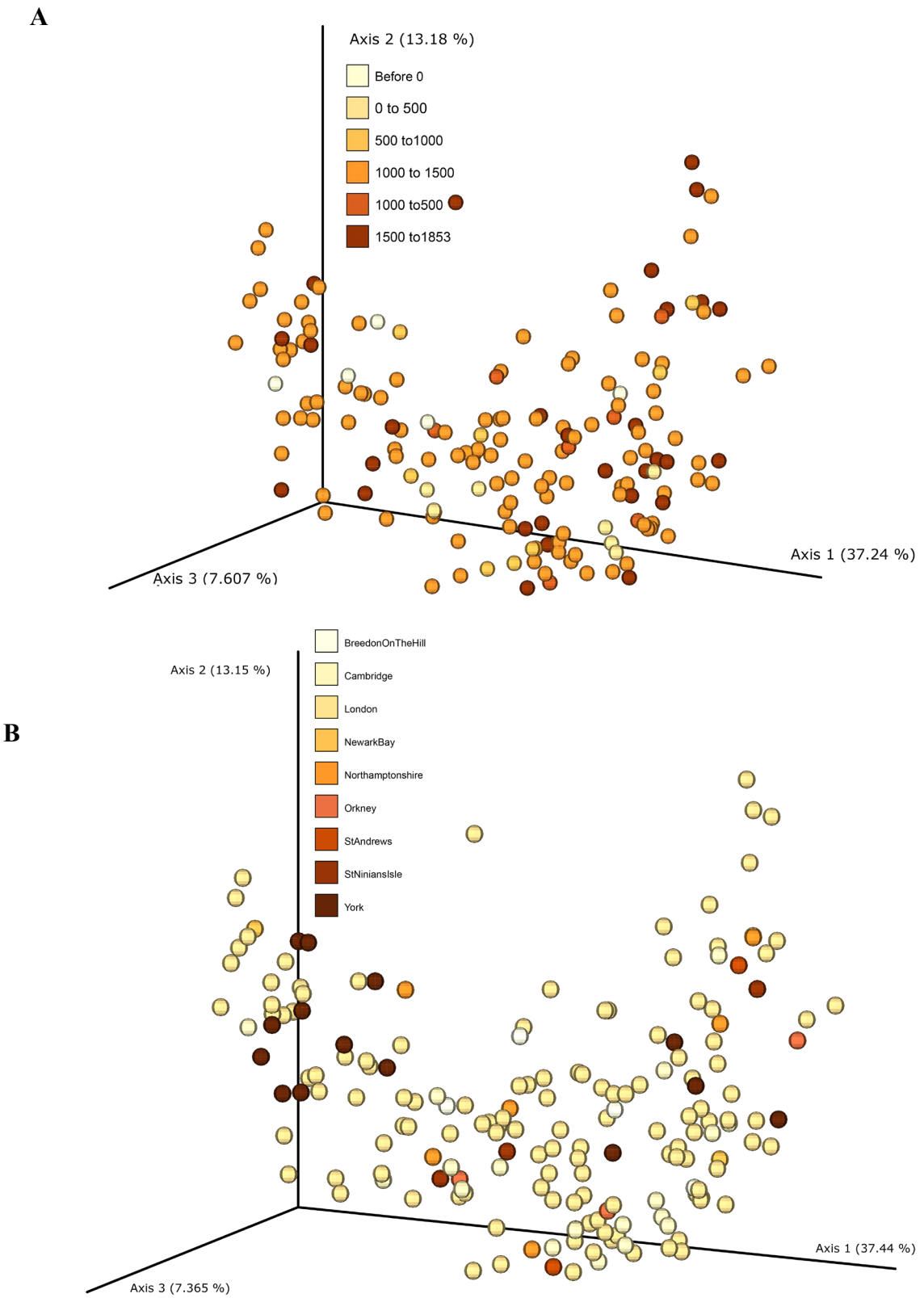

Figure S7: Genus level PCoA plots showing (A) time periods (Before 0, 0 to 500, 500 to 1000, 1000 to 1500, and 1500 to 1853) and (B) geographical regions (Breedon on the Hill, Cambridge, London, Newark Bay, Northampton shire, Orkney, St. Andrews, St. Ninians Isle, and York).

Figure S8: LefSe Analysis of Carnivory and Herbivory Functions

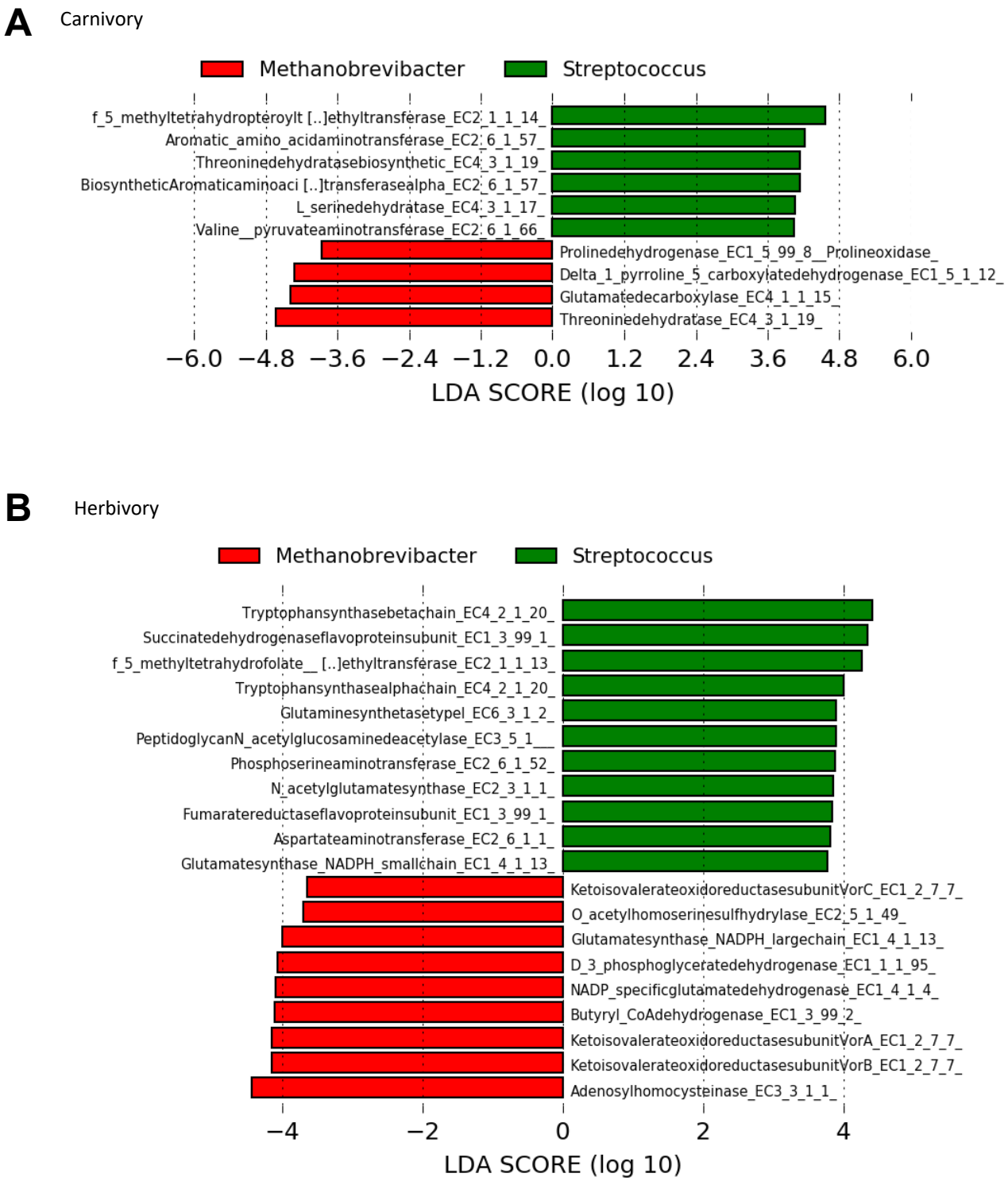

Figure S8: (A) LefSE (Linear discriminant analysis Effect Size) analysis of the *Methanobrevibacter* and *Streptococcus* dominated samples as associated with carnivory functions. (B) LefSE (Linear discriminant analysis Effect Size) analysis of the *Methanobrevibacter* and *Streptococcus* dominated samples as associated with herbivory functions.

Figure S9: LefSe Analysis of Fiber Metabolism Functions

A

High Fiber

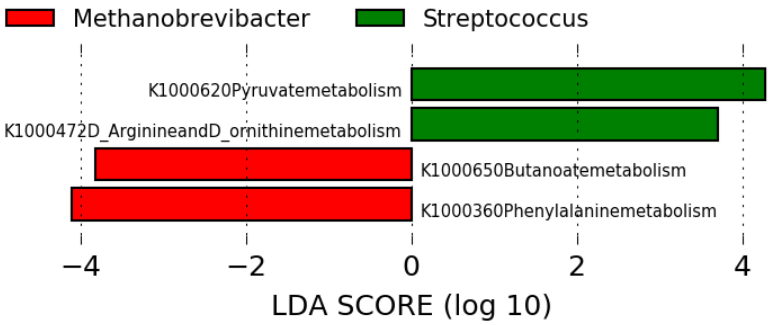

B

Low Fiber

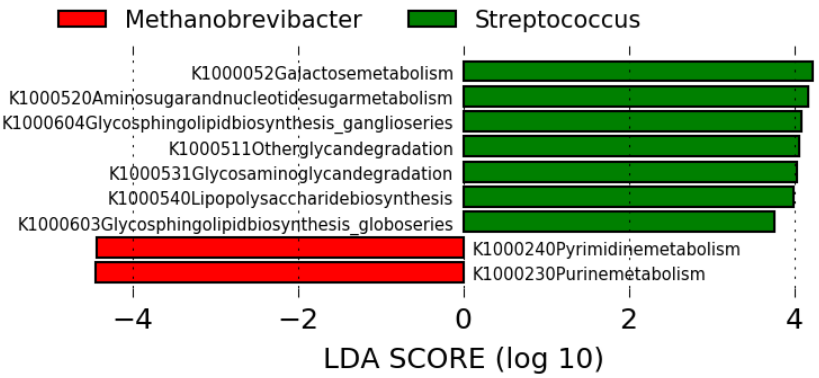

Figure S9: (A) LefSE (Linear discriminant analysis Effect Size) analysis of the *Methanobrevibacter* and *Streptococcus* dominated samples as associated with high fiber functions. (B) LefSE (Linear discriminant analysis Effect Size) analysis of the *Methanobrevibacter* and *Streptococcus* dominated samples as associated with low fiber functions.

Figure S10: LefSe Analysis of Carbohydrate Metabolism Functions

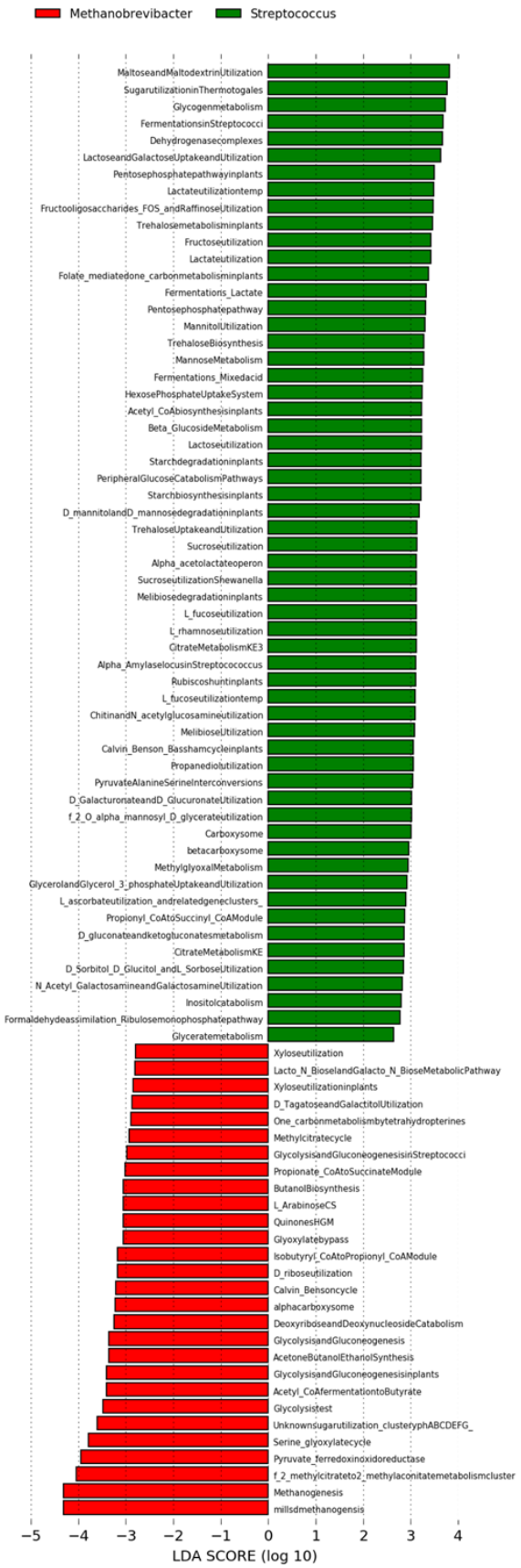

Figure S10: LefSE (Linear discriminant analysis Effect Size) analysis of the *Methanobrevibacter* and *Streptococcus* dominated samples as associated with carbohydrate (sugar) functions.

Figure S11: LefSe Analysis of Dairy Metabolism Functions

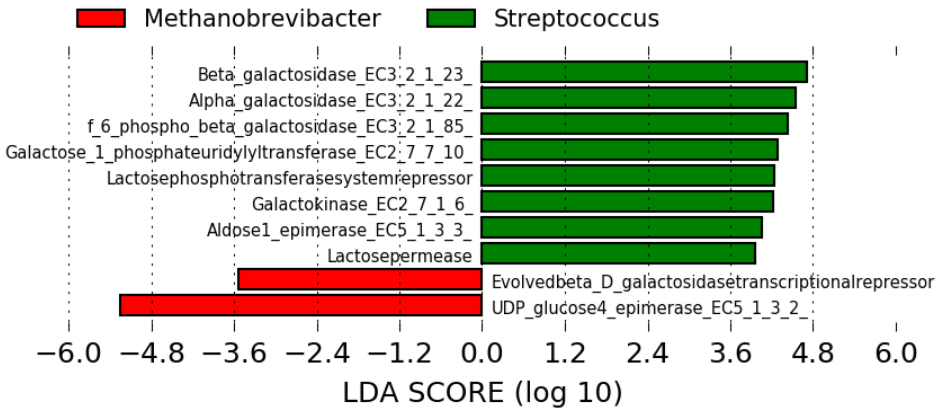

Figure S11: LefSe (Linear discriminant analysis Effect Size) analysis of the *Methanobrevibacter* and *Streptococcus* dominated samples as associated with diary functions.

Figure S12: Community Types Through Time

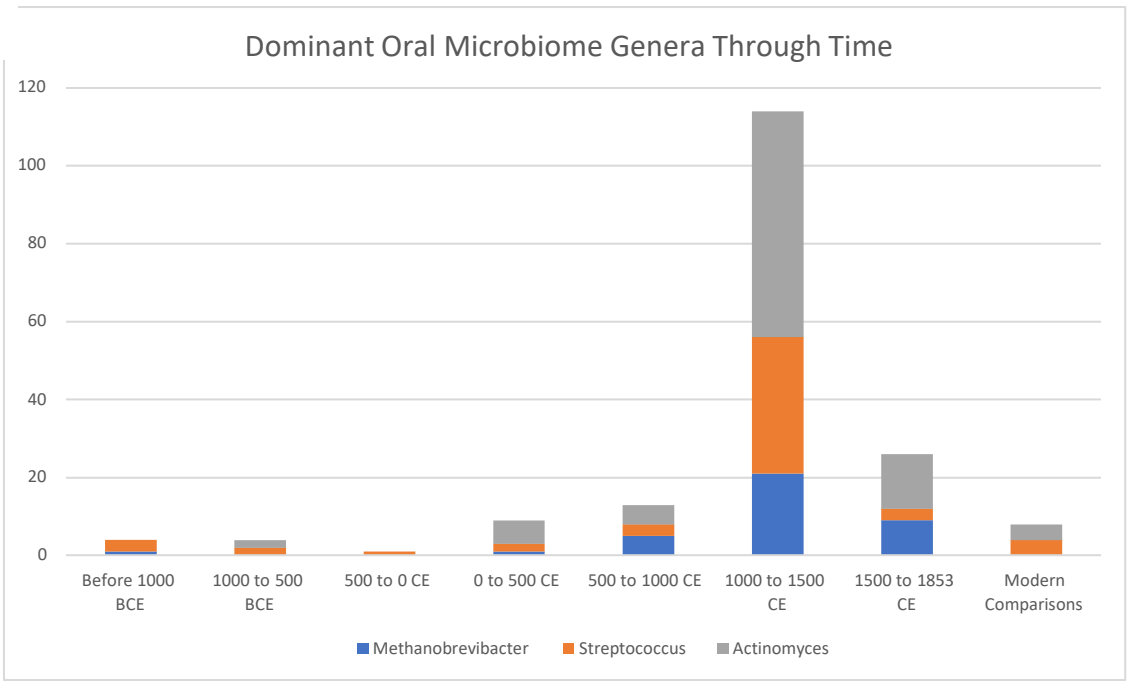

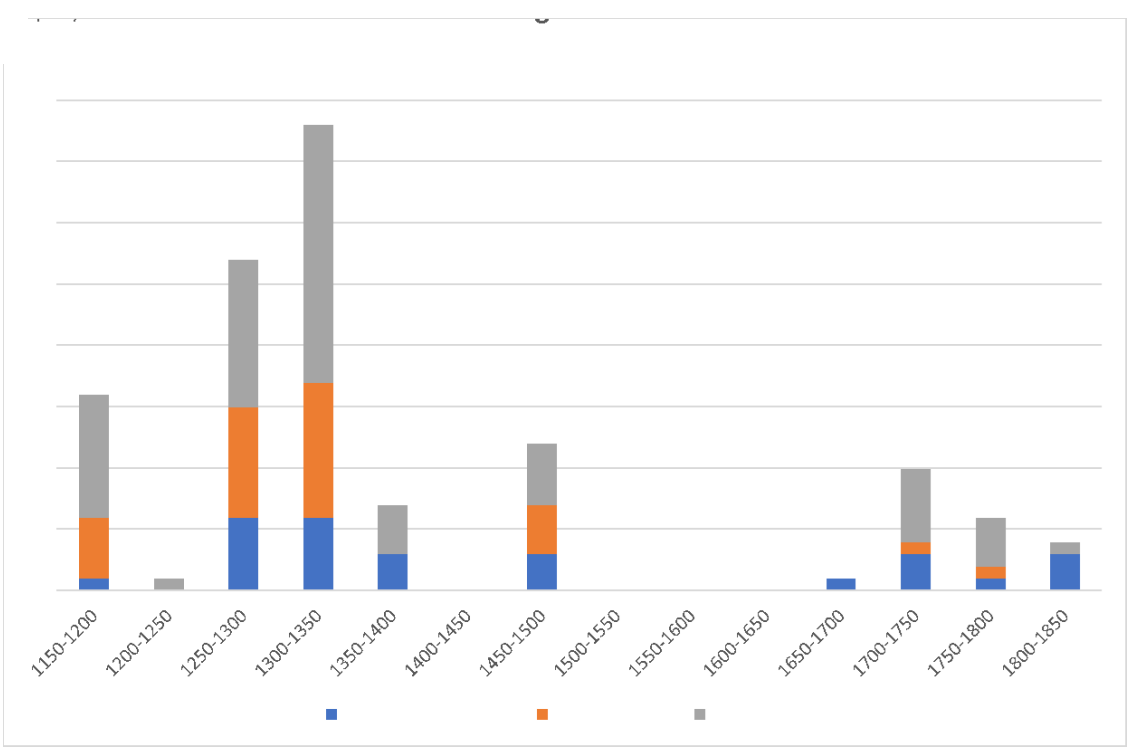

Figure S12: (A) The number of microbial communities dominated by either *Streptococcus, Methanobrevibacter,* or *Actinomyces* are plotted through time, according to their earliest possible date. (B) The number of microbial communities dominated by either *Streptococcus, Methanobrevibacter,* or *Actinomyces* from London, plotted over time according to their median date.

Figure S13:MALTn SourceTracker Analysis

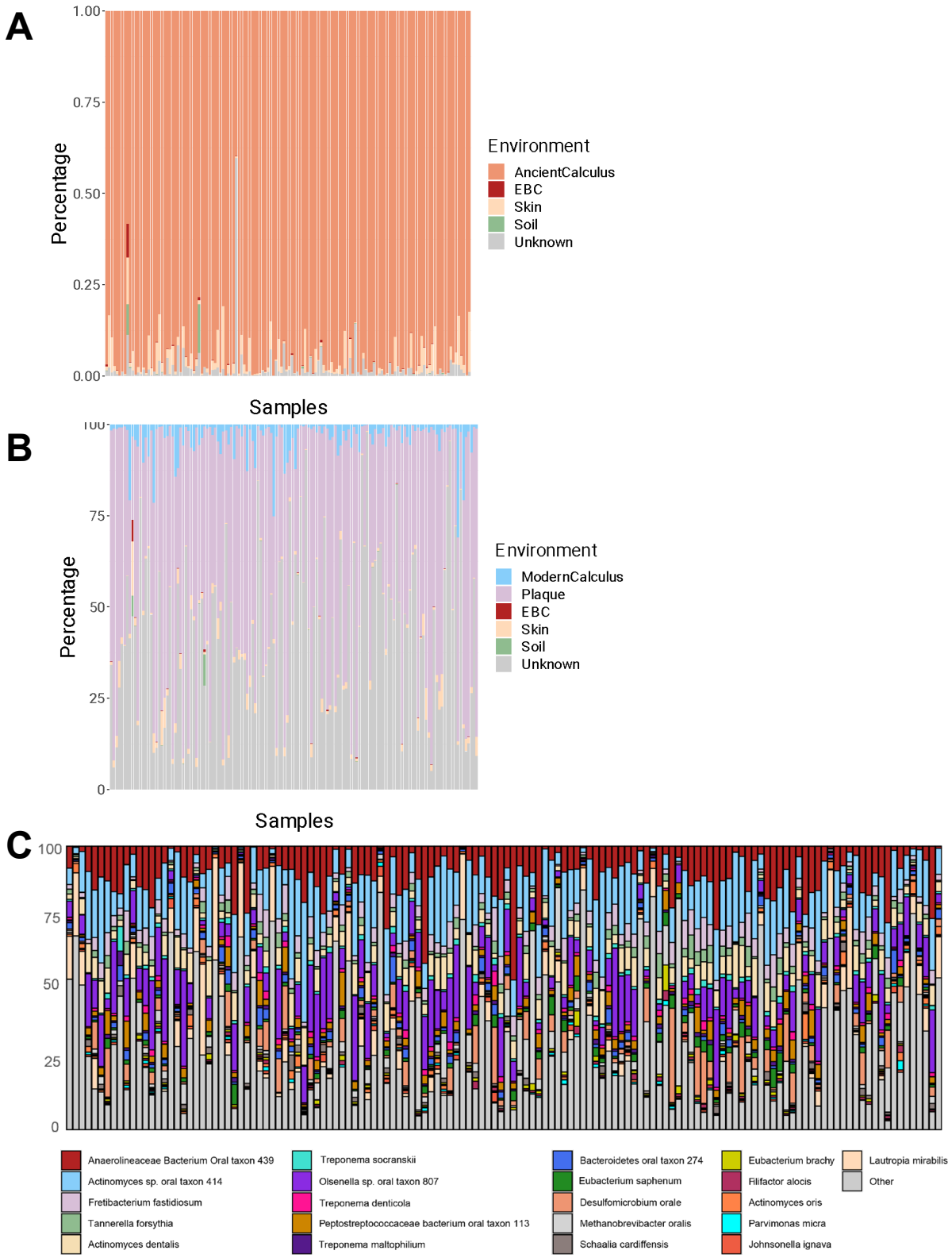

Figure S13: (A) SourceTracker (v2.1.0) results using a genus-level taxon table generated from shotgun sequencing data. The estimated proportions of a sample resembling one of our five environments or from an unknown source. Overall, the archaeological dental calculus samples have the most similarity to those of dental plaque from non-diseased patients. (B) SourceTracker (v2.1.0) results using a genus-level taxon table generated from shotgun sequencing data. (C) A stacked barplot of the taxa present in at least 80 samples at >5% abundance; each of these taxa were also cross validated as present in the Human Oral Microbiome Database (HOMD; accessed on 1/15/2023).

Figure S14: Procrustes Analysis of MALTn versus MALTx Results

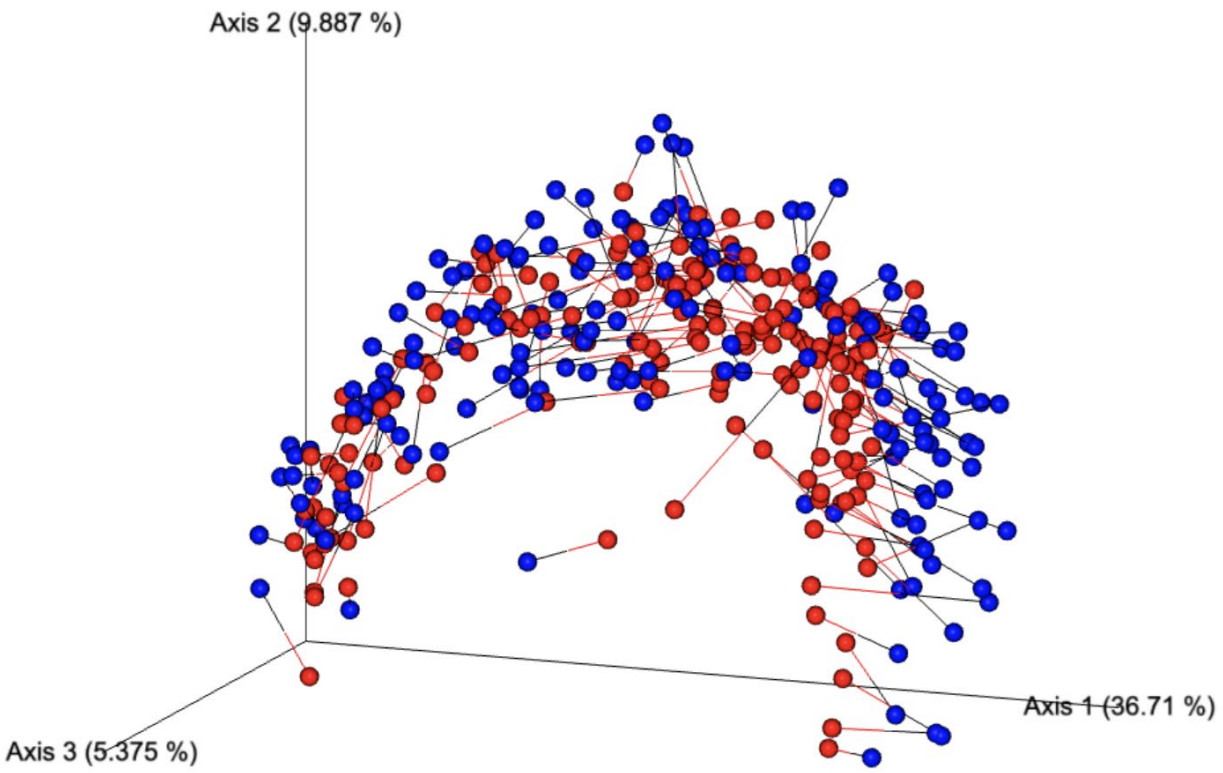

Figure S14: Procrustes plot of the MALTn and MALTx distance matrices (Jaccard) with all taxa-levels included. A mantel test of these results showed a Spearman rho of 0.665231 and a p-value of 0.001.

Figure S15: ALDEX2 Results for Diet-Associated Functions

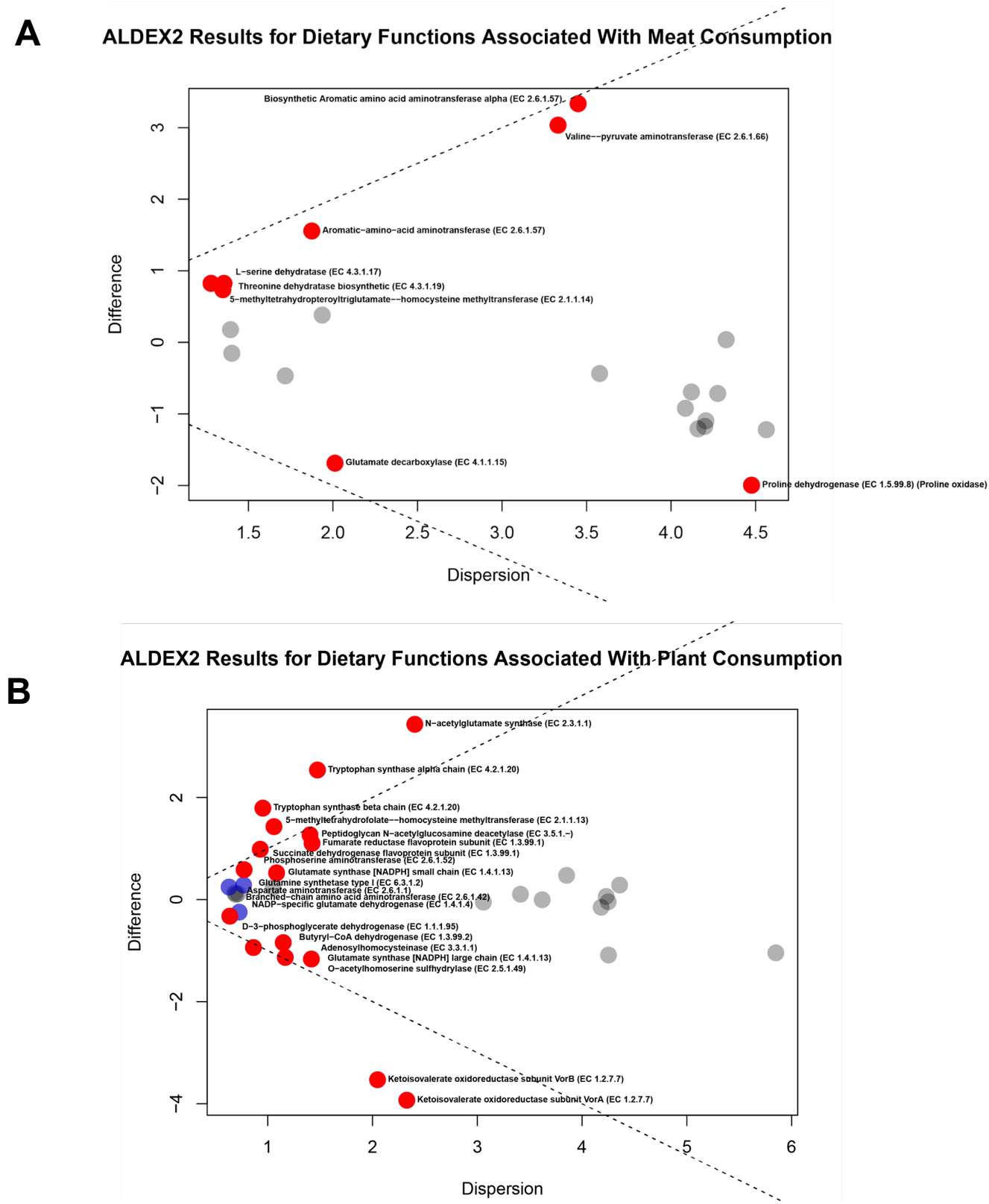

Figure S15: ALDEX2 analyses of the *Methanobrevibacter* and *Streptococcus* dominated samples as associated with dietary functions (A, meat; B, plants; C, dairy; D, sugar; E, high fiber; F, low fiber) using BH-corrected Welch's t-test and Wilcoxon rank test. Features identified by both tests shown in red. Features identified by only one test are shown in blue dots. Non-significant features represent rare features if black and abundant features if grey.

Figure S15: ALDEX2 Results for Diet-Associated Functions

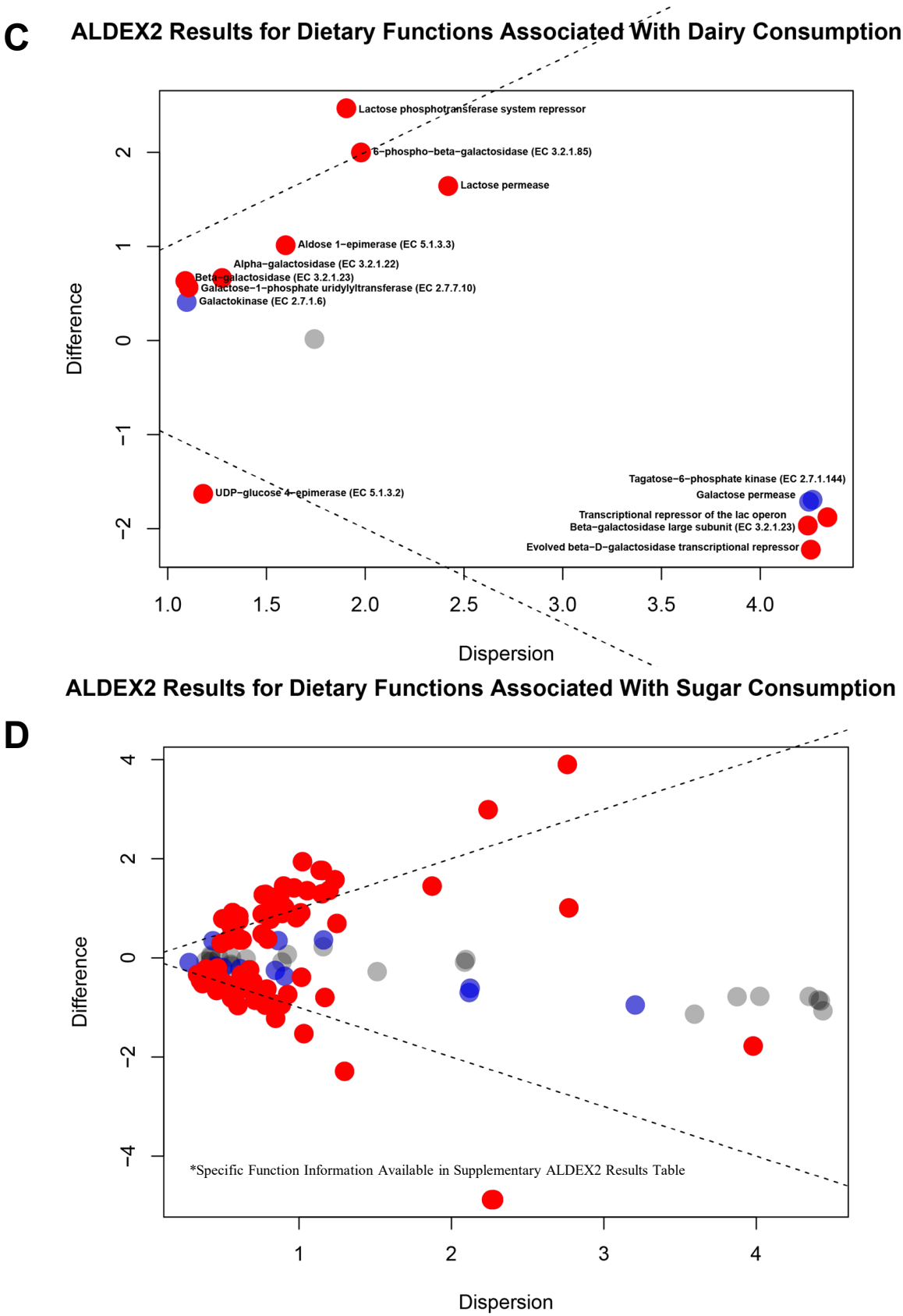

Figure S15: ALDEX2 analyses of the *Methanobrevibacter* and *Streptococcus* dominated samples as associated with dietary functions (A, meat; B, plants; C, dairy; D, sugar; E, high fiber; F, low fiber) using BH-corrected Welch's t-test and Wilcoxon rank test. Features identified by both tests shown in red. Features identified by only one test are shown in blue dots. Non-significant features represent rare features if black and abundant features if grey.

Figure S15: ALDEX2 Results for Diet-Associated Functions

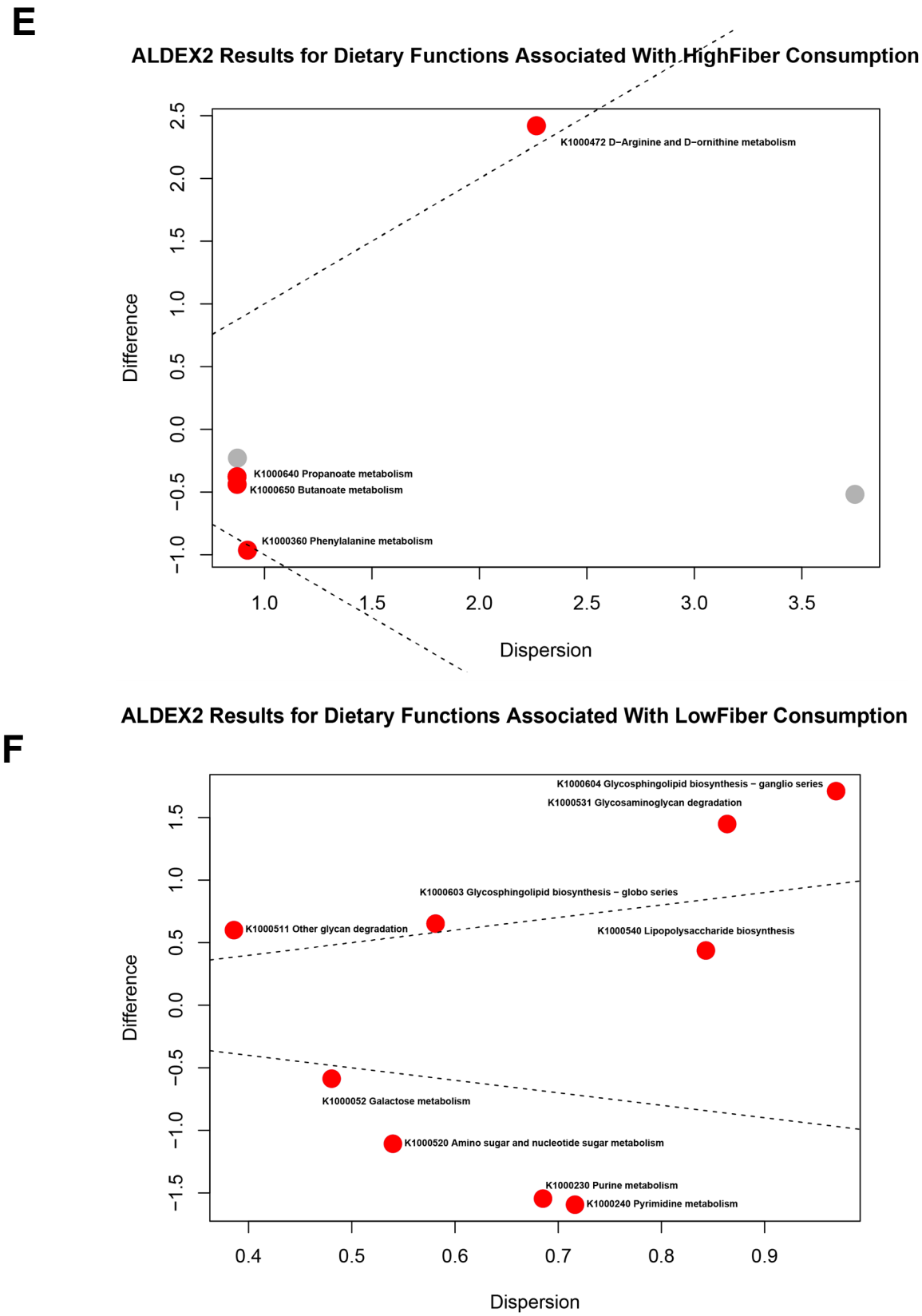

Figure S15: ALDEX2 analyses of the *Methanobrevibacter* and *Streptococcus* dominated samples as associated with dietary functions (A, meat; B, plants; C, dairy; D, sugar; E, high fiber; F, low fiber) using Welch's t-test and Wilcoxon rank test. Features identified by both tests shown in red. Features identified by only one test are shown in blue dots. Non-significant features represent rare features if black and abundant features if grey.

Figure S16: Co-Occurrence Heatmap of Genera

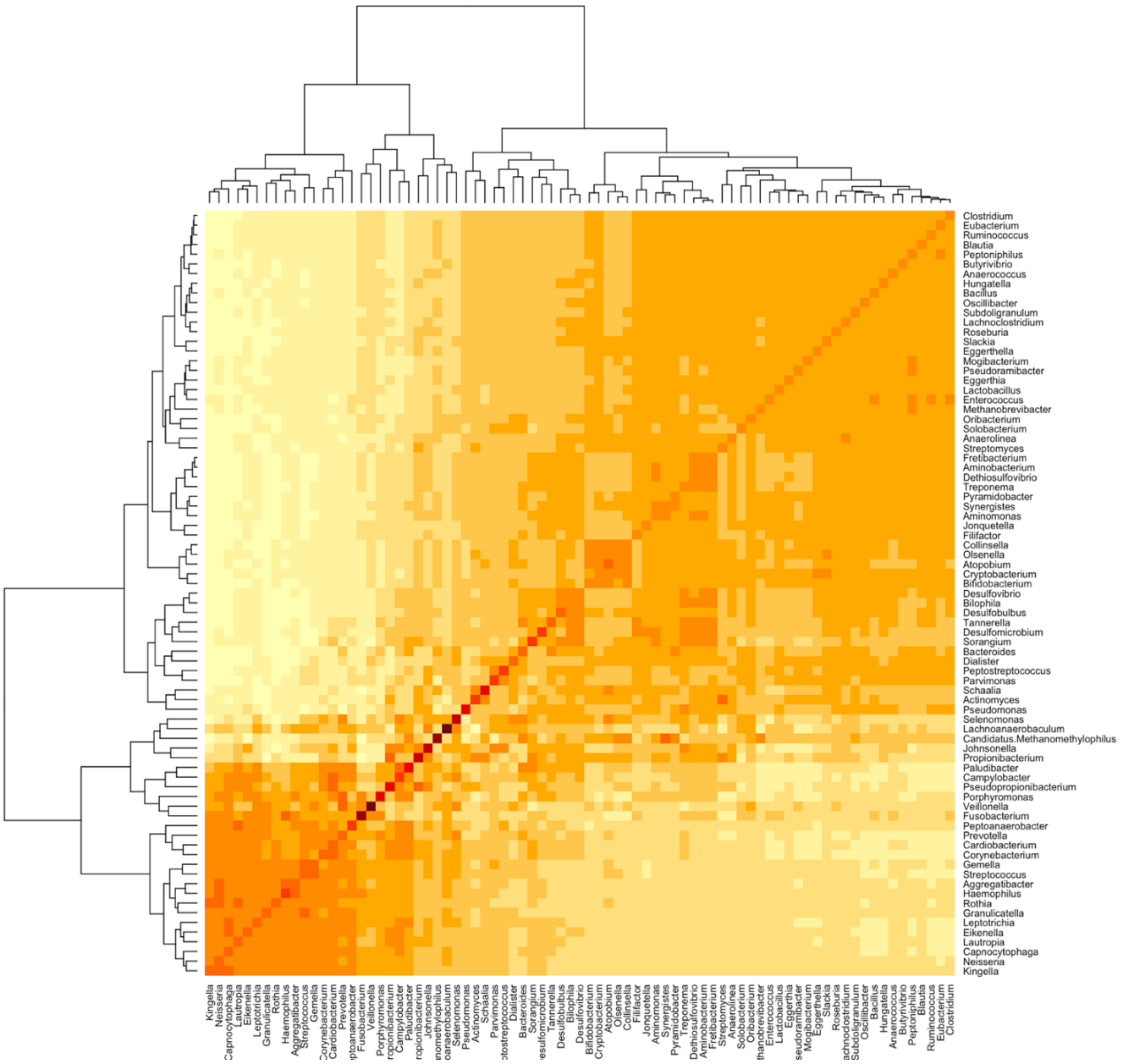

Figure S16: A co-occurrence heatmap at the genera level of the top 70 most abundant genera using Spearman rho coefficients.

Figure S17: Aldex2 results for Significant variables from Table 1

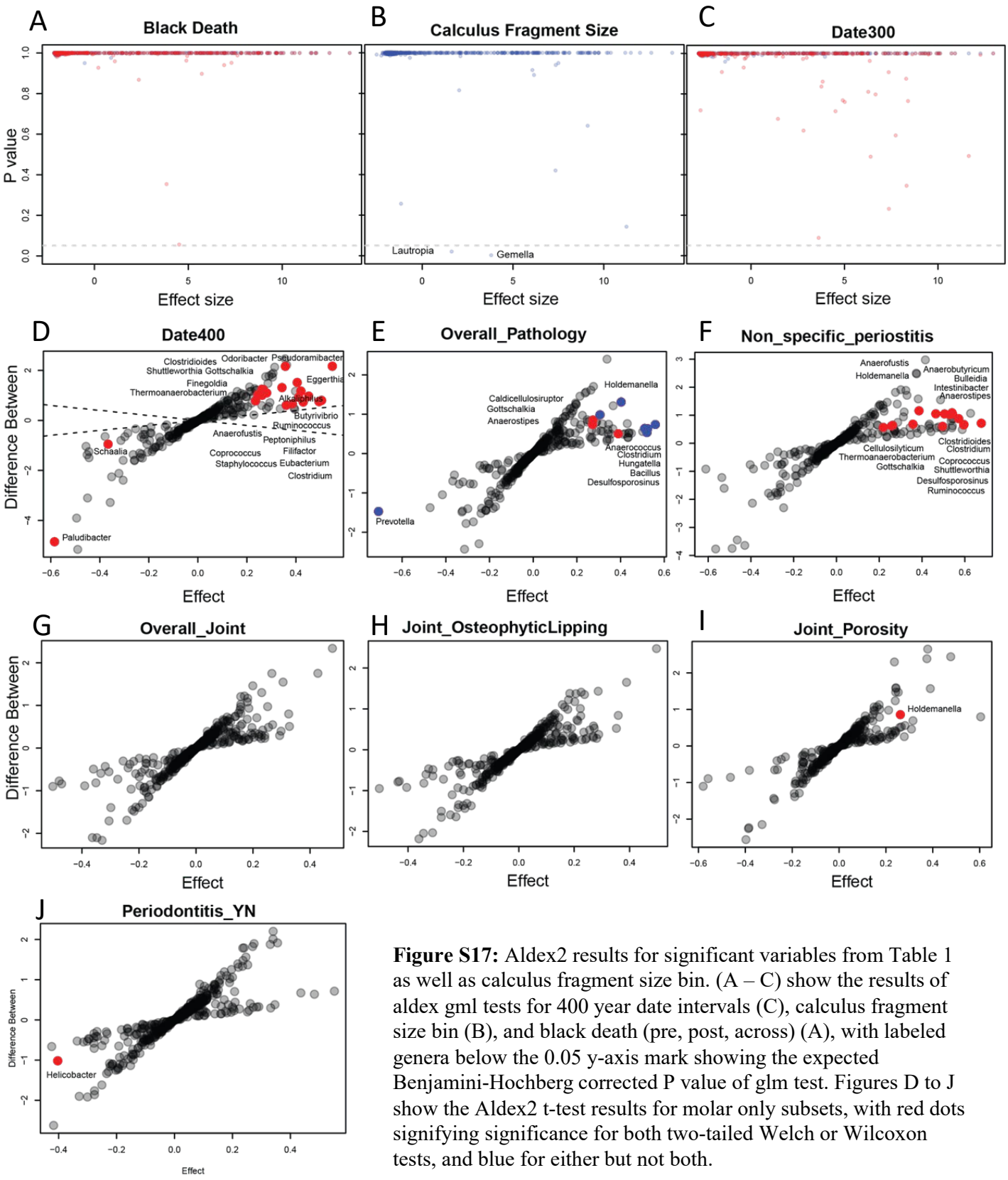

Figure S17: Aldex2 results for significant variables from Table 1 as well as calculus fragment size bin. (A – C) show the results of aldex gml tests for 400 year date intervals (C), calculus fragment size bin (B), and black death (pre, post, across) (A), with labeled genera below the 0.05 y-axis mark showing the expected Benjamini-Hochberg corrected P value of glm test. Figures D to J show the Aldex2 t-test results for molar only subsets, with red dots signifying significance for both two-tailed Welch or Wilcoxon tests, and blue for either but not both.

Figure S18: PCoA of Genus Comparing Mixed vs Distinct Dentition

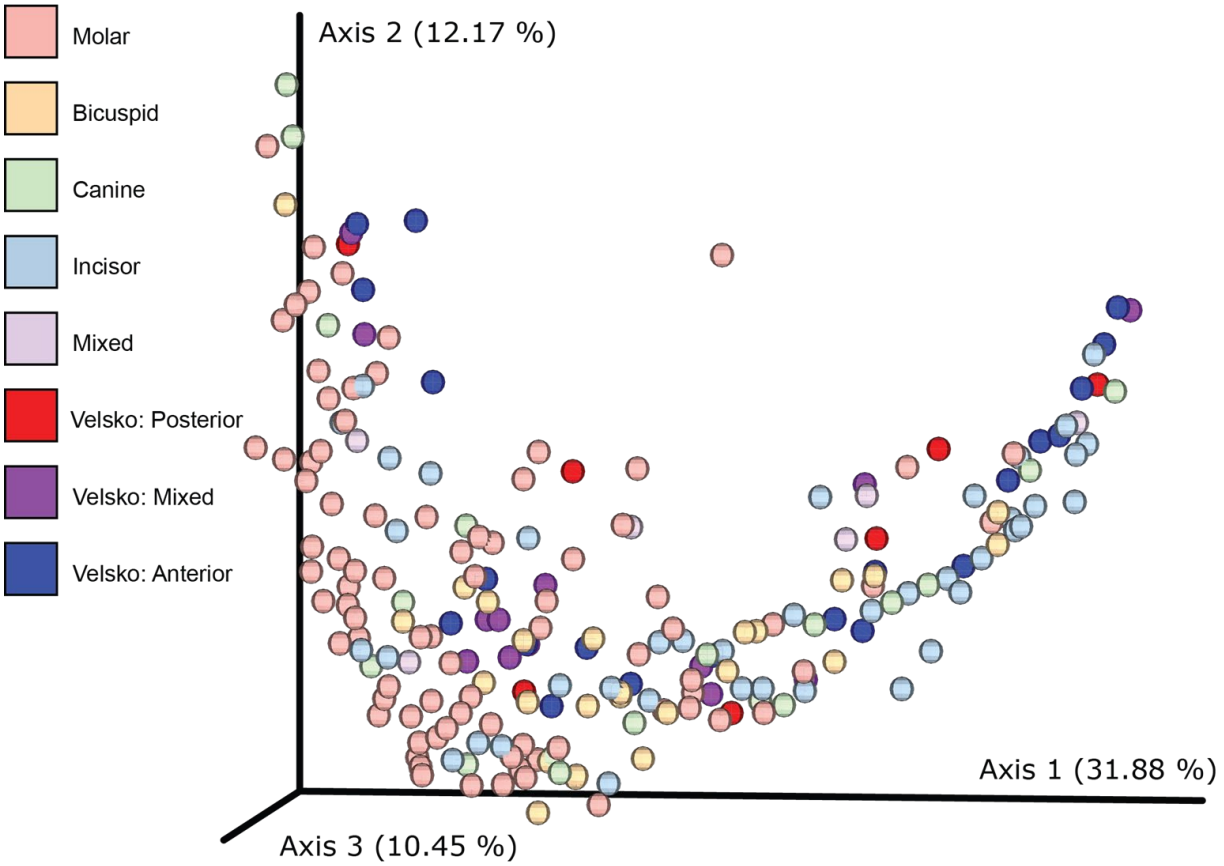

Figure S18: A Principal Coordinates of Analysis (PCoA) plot of Bray Curtis distances of taxa at the genus level comparing samples with distinct or mixed tooth origin for this and the Velsko 2019 publication.

Figure S19: Reads Density Plot (Genus-Level)

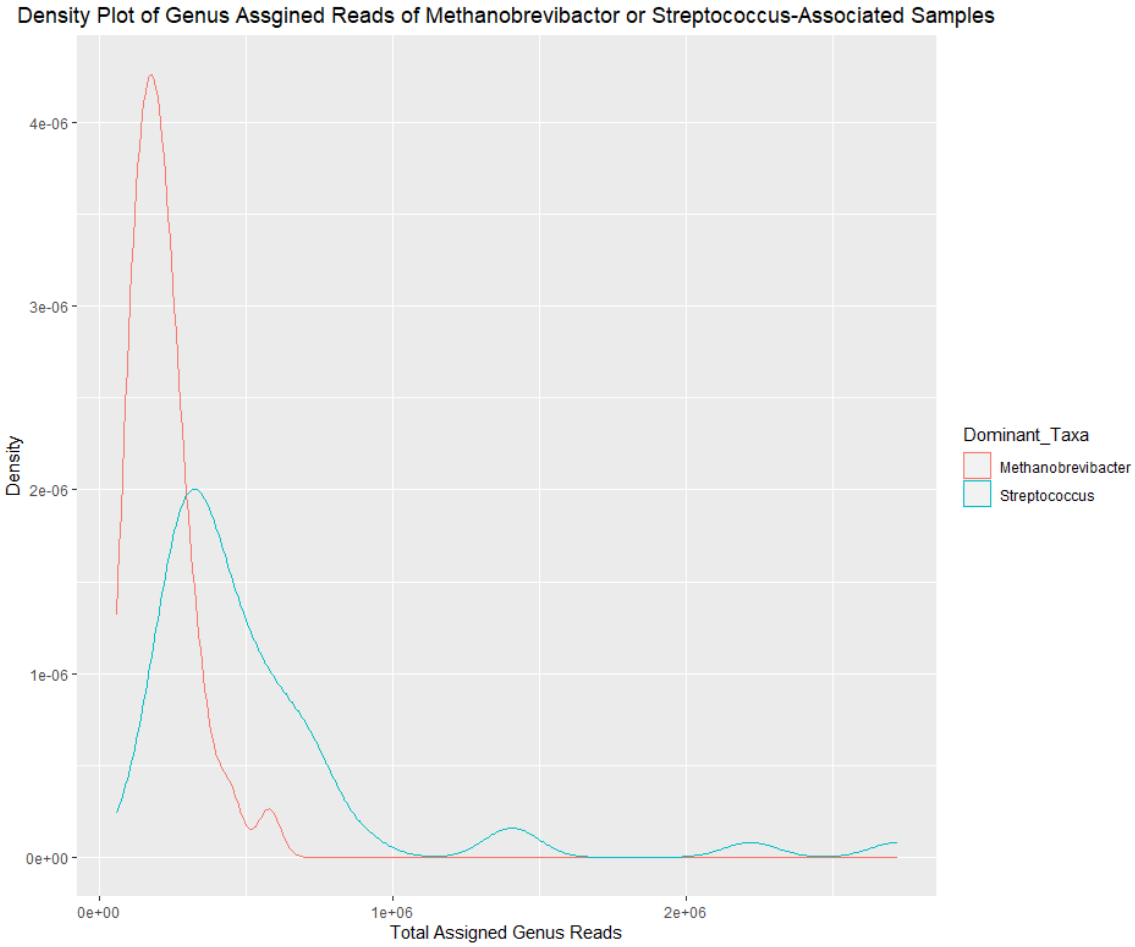

Figure S19: A density plot of genus-assigned DNA sequences within samples that were assigned as *Methanobrevibacter*- or *Streptococcus*-associated.